AD-A153 618 AN EXPERIMENTAL STUDY OF THE PRESSURE IN A FAST BOTTOM BENEATH THE APEX OF AN OVERLYING FLUID WEDGE(U) NAVAL POSTGRADUATE SCHOOL MONTEREY CA M K HEDRICK DEC 84 1/1

UNCLASSIFIED F/G 20/1 NL

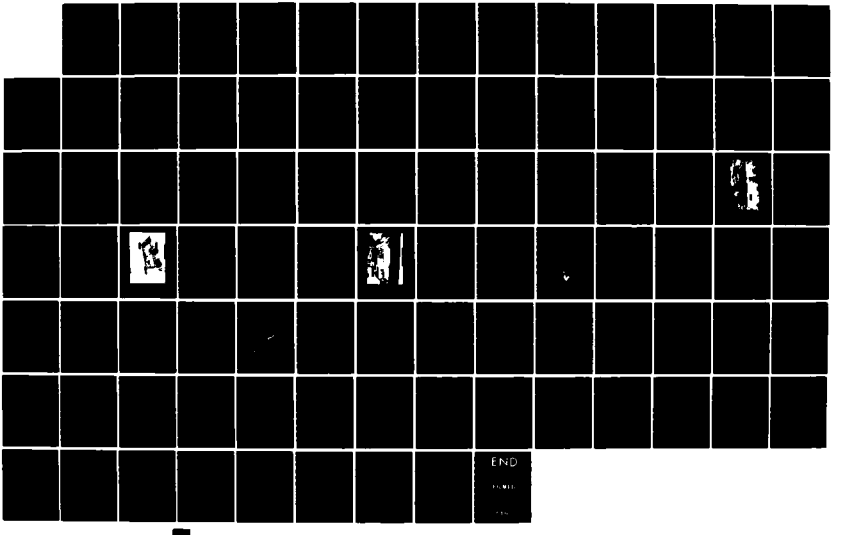

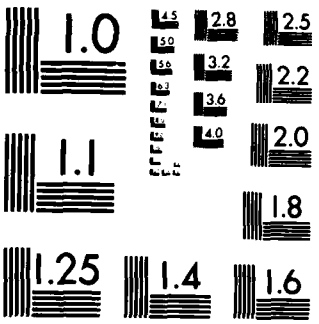

(2)

NAVAL POSTGRADUATE SCHOOL
Monterey, California

THESIS

AN EXPERIMENTAL STUDY OF THE PRESSURE IN A FAST BOTTOM BENEATH THE APEX OF AN OVERLYING FLUID WEDGE

by

Michael K. Hedrick

December 1984

Thesis Advisor: J. V. Sanders

UNCLASSIFIED

SECURITY CLASSIFICATION OF THIS PAGE (When Data Entered)

REPORT DOCUMENTATION PAGE		READ INSTRUCTIONS BEFORE COMPLETING FORM
1. REPORT NUMBER	2. GOVT ACCESSION NO. AD-A153 618	3. RECIPIENT'S CATALOG NUMBER
4. TITLE (and Subtitle) An Experimental Study of the Pressure in a Fast Bottom Beneath the Apex of an Overlying Fluid Wedge		5. TYPE OF REPORT & PERIOD COVERED Master's Thesis December 1984 6. PERFORMING ORG. REPORT NUMBER
7. AUTHOR(s) Michael K. Hedrick		8. CONTRACT OR GRANT NUMBER(s)
9. PERFORMING ORGANIZATION NAME AND ADDRESS Naval Postgraduate School Monterey, California 93943		10. PROGRAM ELEMENT, PROJECT, TASK AREA & WORK UNIT NUMBERS
11. CONTROLLING OFFICE NAME AND ADDRESS Naval Postgraduate School Monterey, California 93943		12. REPORT DATE December 1984 13. NUMBER OF PAGES 89
14. MONITORING AGENCY NAME & ADDRESS(if different from Controlling Office)		15. SECURITY CLASS. (of this report) Unclassified 15a. DECLASSIFICATION/DOWNGRADING SCHEDULE

16. DISTRIBUTION STATEMENT (of this Report)

Approved for public release; distribution unlimited.

17. DISTRIBUTION STATEMENT (of the abstract entered in Block 20, if different from Report)

18. SUPPLEMENTARY NOTES

19. KEY WORDS (Continue on reverse side if necessary and identify by block number)

Pressure Field in a Fast Bottom, Fluid Wedge Overlying a Fast Bottom.

20. ABSTRACT (Continue on reverse side if necessary and identify by block number)

The pressure profile in a fast bottom directly beneath the apex of a fluid wedge was investigated experimentally and compared with a computer model, which used saddle-point approximations based on image theory to predict the pressure under varying acoustical and geometrical parameters. Transducer fluid served as the fluid wedge overlying a water substrate. The fluid in the wedge was contained in an enclosed structure and was separated from the substrate by a thin Mylar membrane. The density ratio

DD FORM 1 JAN 73 1473 EDITION OF 1 NOV 65 IS OBSOLETE

S N 0102-LF-014-6601

UNCLASSIFIED

SECURITY CLASSIFICATION OF THIS PAGE (When Data Entered)

#20 - ABSTRACT - (CONTINUED)

was 0.98 and the speed of sound ratio was 0.91. The experiment was conducted at a frequency of 88.2 kHz. Data were taken with the enclosure pressurized and nonpressurized for wedge angles of two through ten degrees, and with projector elevation angles at one-half and one-quarter the wedge angle. The experimental results agreed with theoretical predictions. Additionally, acceptable agreement was achieved between pressurized and nonpressurized conditions.

Approved for public release; distribution is unlimited.

An Experimental Study of the Pressure in a Fast Bottom Beneath the Apex of an Overlying Fluid Wedge

by

Michael K. Hedrick
Lieutenant Commander, United States Navy
B.S., United States Naval Academy, 1972

Submitted in partial fulfillment of the
requirements for the degree of

MASTER OF SCIENCE IN ENGINEERING ACOUSTICS

from the

NAVAL POSTGRADUATE SCHOOL
December 1984

Author: Michael K Hedrick
Michael K. Hedrick

Approved by: James V Sanders
J.V. Sanders, Thesis Advisor

James V Sanders FOR
A. B. Coppens, Second Reader

James V Sanders
James V. Sanders, Chairman,
Engineering Acoustics Academic Committee

John N. Dyer,
Dean of Science and Engineering

ABSTRACT

The pressure profile in a fast bottom directly beneath the apex of a fluid wedge was investigated experimentally and compared with a computer model, which used saddle-point approximations based on image theory to predict the pressure under varying acoustical and geometrical parameters. Transducer fluid served as the fluid wedge overlying a water substrate. The fluid in the wedge was contained in an enclosed structure and was separated from the substrate by a thin Mylar membrane. The density ratio was 0.98 and the speed of sound ratio was 0.91. The experiment was conducted at a frequency of 88.2 kHz. Data were taken with the enclosure pressurized and nonpressurized for wedge angles of two through ten degrees, and with projector elevation angles at one-half and one-quarter the wedge angle. The experimental results agreed with theoretical predictions. Additionally, acceptable agreement was achieved between pressurized and nonpressurized conditions.

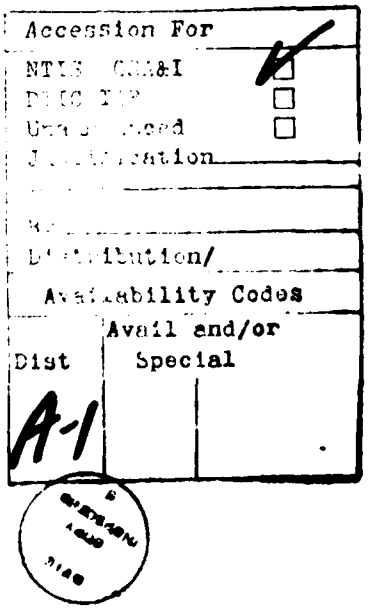

TABLE OF CONTENTS

LIST OF FIGURES

ACKNOWLEDGEMENTS

The author wishes to thank Mr. Bob Moeller for constructing the Fluid Wedge Enclosure and for his encouragement, and Mr. Kerry Yarber, whose technical assistance was most helpful in solving many of the practical problems encountered. Additionally, I would especially like to thank my family for their encouragement and understanding.

I. INTRODUCTION

In a shallow water environment, characterized by a continental shelf, sound energy radiating from a seaward source propagates up the slope toward the shoreline, the apex - the confluence of the water and bottom incline. Assuming isospeed conditions and the absence of reflectors in the water, the energy proceeds towards the apex via rays along a direct path, along rays which reflect from the water-bottom and air-water interfaces, and along rays which refract and diffract. Clearly, the specific paths of the rays are dependent upon acoustical and geometrical conditions which prevail in the shallow water environment. A number of theories, most notably, normal modes, ray, and the method of images, predict that sound energy travelling up a tapered fluid wedge will be transmitted into a fast bottom substrate in distinct beams of sound [Refs. 1,2,3]. Figure 1.1 depicts the fluid wedge geometry.

In 1978, Kawamura and Ioannou [Ref. 4] investigated the acoustic energy transferred from a tapered fluid wedge into a fast fluid bottom. By computing the distribution of pressure amplitude and phase along the interface of the boundary separating the fluids. Comparing their measurements with a model based on a combination of normal modes and ray theory, they accurately predicted the location of the pressure maximum below the apex, but could not account for the structure experimentally found below the depth of maximum pressure. Subsequent effort [Ref. 1] was channelled in the reexamination of the theory in an effort to explain the observed pressure. This examination led to the conclusion that the beams entering the substrate at different distances from the wedge apex interacted causing phase interference,

which produced the structured profile. In general, the pressure increased linearly with depth beneath the apex, peaked, and then experienced a series of pressure minima and maxima. The effort culminated in a computer model, based on image theory, that employed saddle-point approximations to predict the pressure profile beneath the apex. The model predicts the sound field for various acoustical parameters (substrate absorption, densities, and speeds of sound) and geometrical parameters (wedge angle(β) and projector angle (γ)). It was designed for a source at infinite distance, small wedge angles, and small absorption in the substrate. Use of saddle-point approximations restricts the area of validity to a region directly beneath the wedge apex. [Refs. 1,5].

Applying the method of images to the case of a fluid wedge overlying a fast bottom [Refs. 6,7,8], the images lie on a circle with the wedge apex as the center (see Figure 1.2). The images closest to the source correspond to rays which make small grazing angle reflections from the two surfaces of the fluid wedge. The images further from the source correspond to rays with greater angles of elevation or depression. These rays suffer more reflections from the wedge surfaces as they proceed up the wedge and, consequently, experience greater energy loss than the rays represented by the images closer to the source. Assuming smooth wedge surfaces, the complex acoustic pressure is obtained by summing the contributions of the source and the images.

As the rays propagate up the wedge, their angle of incidence increases with each reflection from the surfaces until the grazing angle becomes greater than the critical angle, θ_c, and energy is transferred into the bottom. The closest distance from the apex at which energy is transfered to the substrate is called the dump distance.

$$X = \frac{c}{4 \times f \times \tan(\theta_c) \times \tan(\beta)} \qquad \text{(eqn 1.1)}$$

where:

f = the frequency of the source

θ_c = critical angle ($\cos^{-1}(c_o/c)$)

β = wedge angle

c = speed of sound in the substrate

The experimental model of a slow fluid wedge overlying a fast bottom used in this present research effort was similar to the model used by Kawamura and Ioannou [Ref. 4]. However, this experiment used a much larger and fully enclosed structure capable of being pressurized. Transducer fluid was used in the wedge and tap water served as the fast bottom. The experiment was conducted at a frequency of 88.2 kHz, density ratio (ρ_2/ρ) of 0.98, and speed of sound ratio (c_o/c) of 0.91. Data were taken with the fluid wedge at various angles from two to ten degrees, with the projector at either, one-half or one-quarter the wedge angle. Additional measurements were obtained at wedge angles of four, six, and eight degrees with the fluid wedge enclosure pressurized.

The primary objectives of this experimental research effort were:

A. To determine the fine scale structure of the pressure profile in a fast bottom and to compare the results against theoretical predictions obtained from the computer model.

B. To compare the results obtained when the enclosure was pressurized to the results obtained for similar conditions when the enclosure was nonpressurized.

C. To determine if projector location within the fluid wedge alters the pressure profile for a similar wedge angle and projector depth.

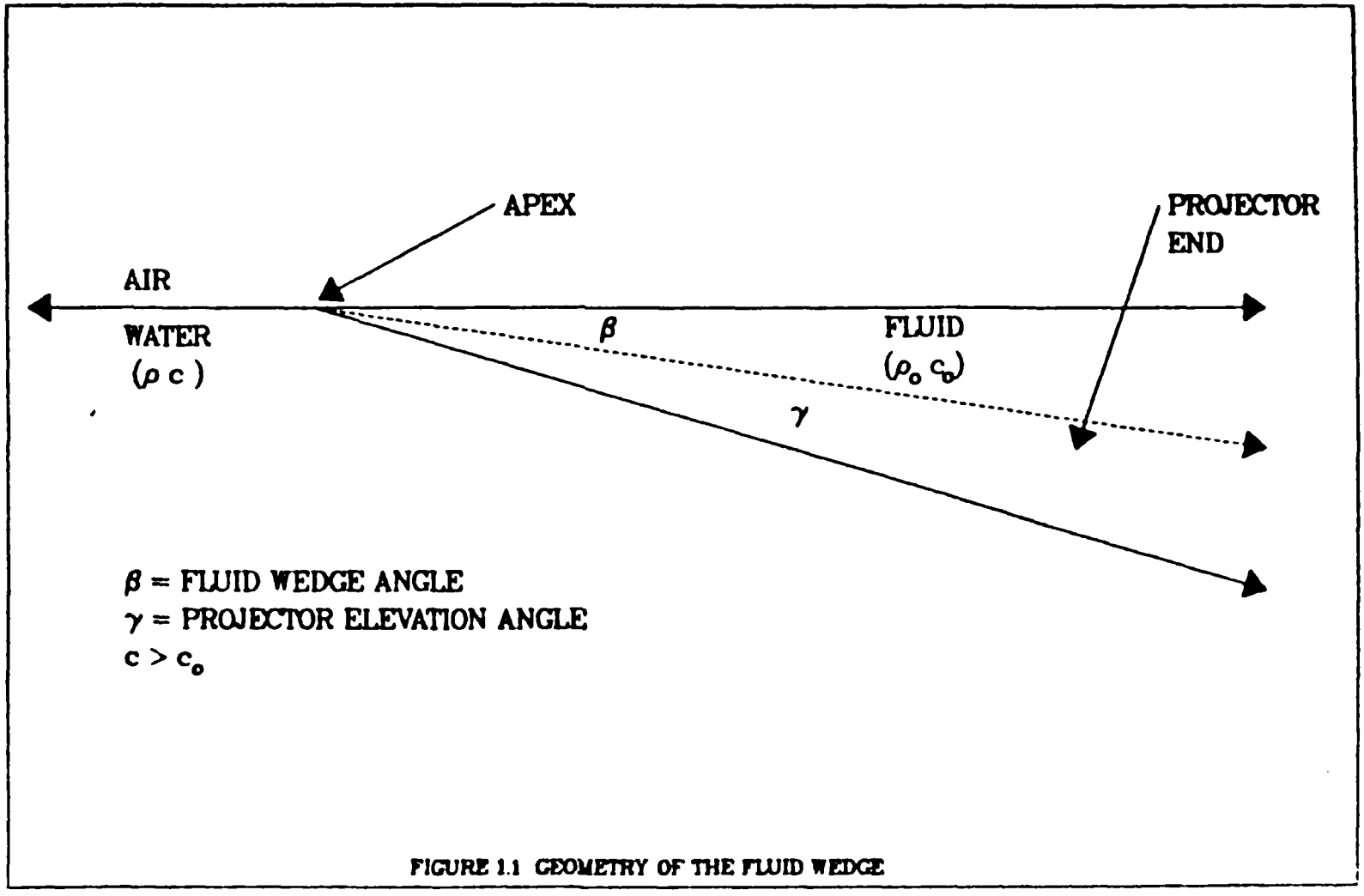

FIGURE 1.1 GEOMETRY OF THE FLUID WEDGE

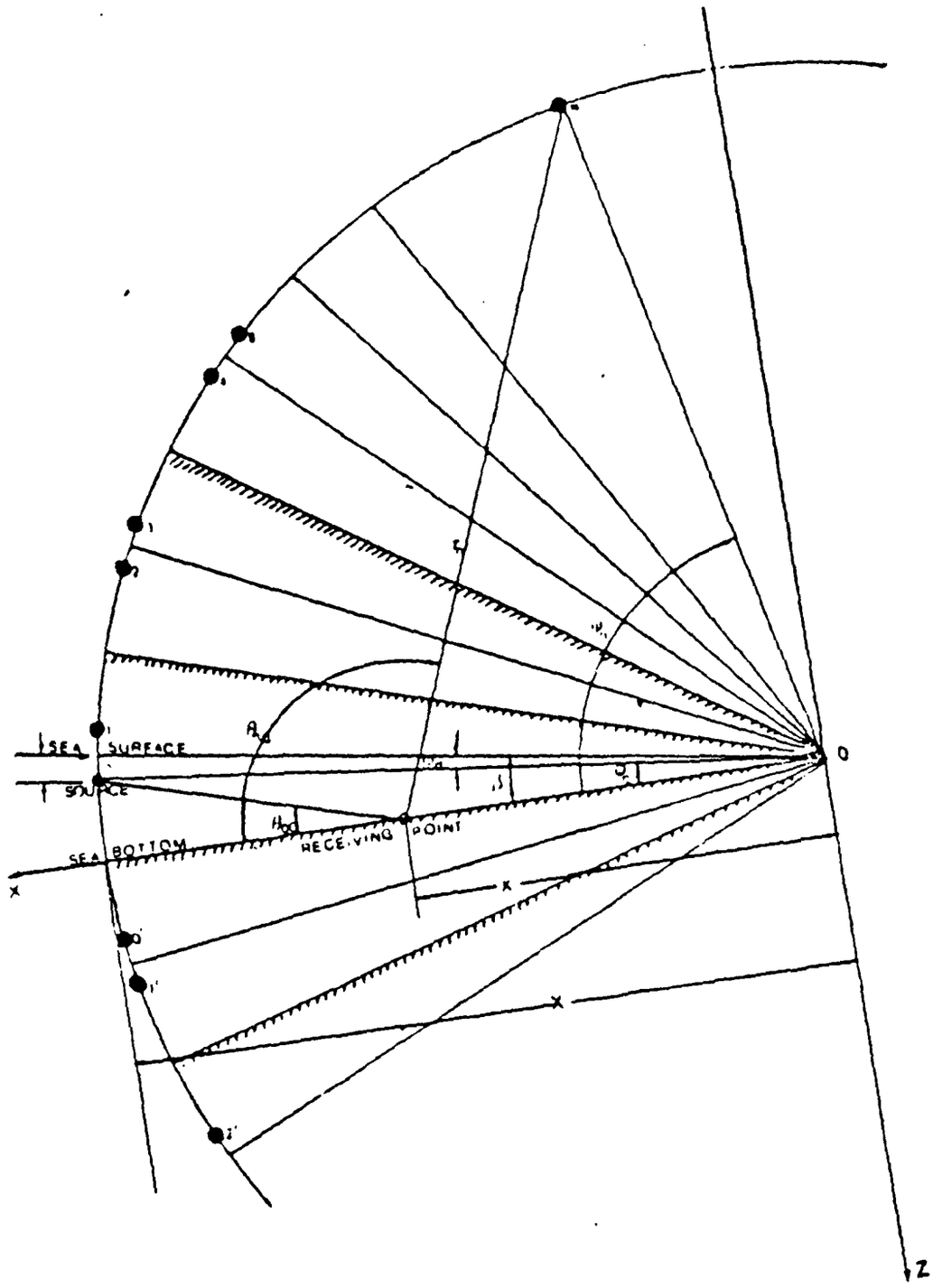

Figure 1.2 Geometry of a wedge by the method of images

II. THEORY

The expression for the pressure in the substrate is derived from the Method of Images, which assumes distant image pairs, in conjunction with Green's Intregal Function [Ref. 1]. The equation for the pressure in a lossy substrate is given as:

$$p(\nu,\eta,t) = (j/4)\exp(j\omega t)\underset{\sim}{k}X \sum_{n=1} A_n \exp(-j\underset{\sim}{k}Xa_n\nu) I_n \qquad \text{(eqn 2.1)}$$

Where:

$$I_n = \int_{(\nu^2+\eta^2)^{1/2}}^{\infty} [\eta/(\lambda^2-\eta^2)^{1/2}]\, H_1^{(2)}(\underset{\sim}{k}X\lambda)\exp(j\underset{\sim}{k}Xa_n(\lambda^2-\eta^2)^{1/2})\,d\lambda$$

$k = k-j = k(1-j\ )$; $K = w/c$

$kX = T / 2(2\text{Tan}\Theta\ \text{Tan}\ )$; $\Theta = \text{Cos}\ (c/c)$

$a = \text{Cos}\Theta / \text{Ccs}\Theta$

Nondimensional factors :

$\nu = -x/X$; $\eta = z/X$; $r = \{(x'/X + \nu)^2 + \eta^2\}^{1/2}$

X = dump distance

β = wedge angle

See Figure 2.1 for wedge geometry and nomenclature.

Equation 2-1 can be further simplified by applying saddle-point techniques, which further restrict the applicability of the final expression. Evanescent, refracted, and diffracted waves are all affected by the constraints imposed by the saddle-point approximations. Equation 2-2 is the resulting equation.

$$p(\nu,\eta,t) = (-1/2)\exp(j\omega t)\left\{\sum_{\theta_n<\theta_c} A_n \exp[jkx\eta(a_n/a_{in})(a_n^2-1)^{1/2}]\exp[-\gamma kx(\nu a_n)] \right. \quad \text{(eqn 2.2)}$$

$$\left. + \sum_{\theta_n>\theta_c} A_n \exp[-\gamma kx(\nu a_n + \eta a_n\sqrt{1-a_n^2}/a_{in})]\, F(\Delta_{in})\right\}$$

WHERE:

$$\Delta_{in} = (kx/\pi)^{1/2} a_n^{-1}(1-a_n^2)^{3/4}\eta^{-1/2}\left[(\nu^2+\eta^2)^{1/2} - \eta/(1-a_n^2)^{1/2}\right]$$

$F(\Delta_{in})$ is a Fresnel Intregal which describes the transition between a diffracted and refracted arrivals.

A convenient case is when ν is allowed to go to zero. THEN, FOR FINITE VALUES OF η, ϕ IS EQUAL TO $\pi/2$. THIS effectively reduces the number of constraints on equation 2-2 to the following:

$$z > \lambda/(\pi \sin\theta_c) \qquad \text{(eqn 2.3)}$$

$$z > \lambda \qquad \text{(eqn 2.4)}$$

This restricts the applicability of equation 2-2 to a depth greater than a wavelength and in the region directly below the wedge apex.

The interested reader should consult reference (1) for the details in the evolution of equation 2-2. Additionally, reference (1) provides similar equations for a lossless substrate and compares the solutions obtained by the saddle-point and the end-point methods.

Equation 2.2 was programmed for a Wang 2000 desk-top computer [Ref. 1] and this program ("WEDGE17") was used in this thesis to predict the pressure in the substrate.

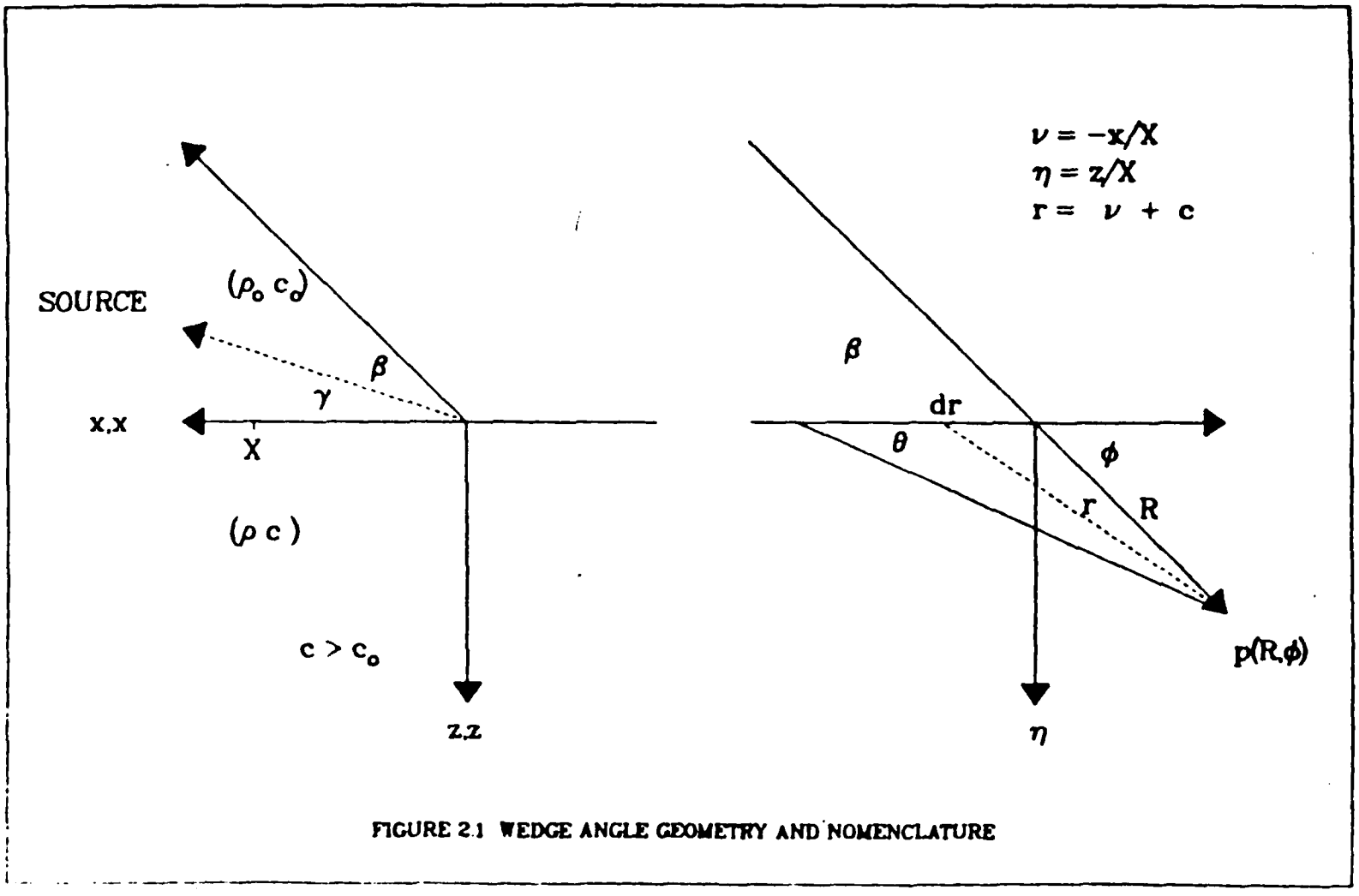

FIGURE 2.1 WEDGE ANGLE GEOMETRY AND NOMENCLATURE

III. EXPERIMENT

A. SUMMARY OF APPARATUS FUNCTIONS

The experimental facility consisted of a rectangular enclosure which contained a wedge of transducer fluid, the slow medium, suspended over a wooden tank filled with tap water, the fast bottom substrate. The two liquids were separated by a thin Mylar membrane. The enclosure could be pressurized by a hand pump through an air control valve on the top of the enclosure. The desired wedge angles were achieved by elevating one end of the enclosure. The projector, located on the longitudinal centerline of the enclosure, was positioned opposite the apex. It transmitted a pulsed signal up the wedge towards the apex. The projector was restricted to two horizontal locations along the longitudinal axis of the enclosure: 87.31 cm and 57.0 cm from the wedge apex. However, at each of those locations the projector could be positioned vertically anywhere within the fluid wedge enclosure. All experimental events except one were conducted with the projector at a distance of 87.31 cm. The transmitted pulsed signal was received by two LC-10 hydrophones; one located in the wedge enclosure and the other in the water tank directly beneath the apex. The received signals were amplified and then measured on the Nicolet oscilloscope. A photograph of the experimental facility is shown in Figure 3.1. Figure 1.1 provides an illustration of the fluid wedge geometry.

B. APPARATUS DESCRIPTION

1. Water Tank

The water tank was one of the tanks available in the underwater acoustics laboratory at the Naval Postgraduate School. The tank was constructed of plywood with the following interior dimensions: length - 70.5 in.; width - 34.5 in.; and depth - 23.75 in. The inside surfaces were painted with Varathane. To reduce bottom reflections, a pad of rubber cone absorbers was placed on the bottom of the tank beneath the apex. The tank was filled with water from a tap at the site. The water temperature remained relatively constant during a given measuring event. However, the temperature ranged from 20.8 to 21.2 degrees Celsius through the entire duration of this study. The water level was maintained at the same height as the top surface of the transducer fluid within the enclosure. Thus, it was necessary to adjust the water level for each increment in the wedge angle. Figures 3.2, and 3.3 are drawings of the water tank and the enclosure.

2. Fluid Wedge Enclosure

The enclosure was a rectangular box constructed of aluminum, plexiglass, and Mylar components. The enclosure is shown in Figure 3.4. Its dimensions were as follows: length - 37.0 in.; width - 16.0 in.; and height - 8.5 in. It was fabricated of 0.5 in. thick aluminum sidewalls, 0.5 in. thick plexiglass top, and a 0.5 mil thick Mylar bottom membrane.

On the interior side of the backwall (projector end) five lines were etched which corresponded to the fluid levels necessary to achieve wedge angles of two, four, six, eight, and ten degrees. Additionally, two strips of measuring tape, graduated in millimeters, were placed on the

backwall from the Mylar bottom to the plexiglass top. This provided a means of determining the fluid depth for wedge angles other than those listed above. Additionally, the backwall contained a 0.75 in. diameter drain port which was used to drain the fluid from the enclosure upon completion of the experiment. A compass-rose (protractor head) and brass weight assembly was attached to the right sidewall near the apex. The compass-rose could be read to one-twelfth of a degree. Unfortunately, the assembly proved to be less reliable than intended, thus it provided only rough estimates of the wedge angle. Inside of the wedge enclosure, four cylindrical aluminum strength members were installed perpendicular to the long aluminum sidewalls. They were equally spaced along the length of the sidewalls and on a ten degree incline from the apex frontwall to the projector backwall. The starting point of the incline was placed 1.0 in. above the wedge apex so that at no time would the strength members make contact with the fluid wedge. The strength members were installed to maintain the designed distance between the long sidewalls while under tension from the stretched Mylar. Previous work [Ref. 4] indicated that the tension in the Mylar caused the sidewalls to bend inward. The strength members served their purpose.

A plexiglass top was selected to allow the depth of the fluid wedge to be observed and to allow the depth of the fluid wedge, Projector A, and Receiver A to be measured. The top contained four access openings which were designated A,B,C, and D. The first three access openings were cut along the longitudinal centerline while access D was off-center at the projector end of the enclosure. Access A was designed to hold an LC-10 hydrophone, Receiver A. This receiver's purpose will be discussed in subsection 4. Access B served as the main fluid inlet port and as the position for the projector during the final event of the

experiment. Access C served as the projector access for all events, except one. Access E contained the air control valve used for pressurizing and decompressing the fluid wedge enclosure. Accesses B, C, and D were fitted with circular plexiglass cover plates that were grooved on the interior face. A rubber "O" ring was inserted in the groove. The cover plates were fitted with four to six screws, which held them in postion while exerting pressure on the "O" ring to produce an airtight seal of the access. Access A and the cover plate for Access C contained similar brass fittings that pierced the plexiglass and locked in position the shafts of Receiver A and Projector A respectively. The fittings consisted of an exterior threaded coupling with a bored threaded nut. Inside of the nut were two tapered nylon bushings. The opening through the fittings was made airtight by tightening the nut down upon the coupling, forcing the nylon bushings to collapse around the inserted shaft. Use of flexible nylon bushings allowed the fittings to be adjusted repeatedly during the experiment without fear of compromising the airtight integrity of the fluid wedge enclosure. When the projector was shifted forward to Access B the two cover plates were simply interchanged. This minimized the number of fittings required for the enclosure.

A thin Mylar membrane was selected to provide an acoustically transparent membrane between the liquids. Before the Mylar could be attached to the bottom of the enclosure, it was necessary to stretch it as tight and flat as possible to minimize all surface irregularities and bowing. The stretching was accomplished in a two-step operation. First, the Mylar was stretched and taped down to the flat glass top of a mechanical drawing table. Ordinary masking tape did an excellent job in holding the mylar in place. Ninety-five percent of all the wrinkles in the Mylar

were eliminated during this step. The second step employed a wooden Mylar stretcher mechanism which further stretched the Mylar longitudinally and laterally by pulling handles connected to free moving arms that rode on the stretcher's guiderails. Figure 3.5 is a photograph of the Mylar strecher. Royal Bond Grip, a water resistant glue that must be applied to both surfaces beiny bonded, was brushed on the bottom of the stretcher's perimeter, the longitudinal and lateral arms, and on the corresponding areas of the Mylar. After allowing the Grip to dry for approximately 10 minutes, the stretcher was placed on the Mylar. Weights were placed on the arms and around the perimeter of the stretcher to provide additional pressure on critical areas. The Grip was allowed to cure for six hours. The Mylar was then ready to be stretched by the arms. The bottom of the arms, which now were glued securely to the Mylar, were allowed to travel in their directions by sliding along the glass top of the table and guiderails of the stretcher. The weights were then removed from the arms which were subsequently pulled separately approximately 0.5 inches in each direction until the Mylar was fully stretched and presented a "mirror-like" surface. To prevent slipping under the increased tension, the arms were locked into position with wing nuts and the weights reapplied. The stretcher successfully stretched the Mylar approximately three inches further than achieved in step one.

The bottom of the enclosure and a strip one inch wide around the aluminum sidewalls were sanded to provide a rough surface for the Grip which was subsequently applied to those areas. Before applying Grip to the desired area on the Mylar, a pattern was made of the 36 in. by 15 in. interior bottom area of the enclosure. The pattern was then placed on the Mylar as a guide for applying the Grip on that surface. Once the Grip dried, the fluid wedge enclosure was

placed on the Mylar with particular care to ensure that the glued bottom of the enclosure matched-up with the glued rectangle on the Mylar. Additional weights were placed on the top of the enclosure and the Grip was allowed to cure for 24 hours.

At the end of the curing period, the Mylar was cut approximately one inch from the enclosure with a razor blade. The enclosure was then lifted so that it rested on its front sidewall in a vertical orientation. With the enclosure in this position, Grip was applied to the one inch of excess Mylar around the enclosure and to the previously sanded areas of the aluminum walls. After the Grip dried, the excess Mylar was pulled tightly and then glued to the walls of the enclosure. The excess Mylar provided an extra margin of safety in the event that the Mylar glued directly to the 0.5 in. border of the enclosure's bottom gave way as a result of the upward force of the water, the weight of the tranducer fluid, or the enclosure's pressurization.

Upon completion of the Mylar installation, two aluminum arms were attached to the enclosure which allowed the enclosure to be suspended over the water tank. The short pivot arm was attached to the backwall (projector end). The arm was connected to a short length of angle iron that fit over the interior lip of the water tank. The angle iron had one set screw at each end that could be adjusted to level the enclosure. The long arm was attached to the frontwall (apex end) and extended to a horizontal bar assembly at the opposite end of the water tank. The desired wedge angles were achieved by raising the horizontal bar, thus lifting the long arm and forcing the fluid wedge enclosure to pivot on the short arm. The long arm also contained a receiver assembly which controlled the positioning of Receiver B, an LC-10 hydrophone, in the water tank beneath the apex of the fluid wedge.

3. Projector A

The transmitter was required to have a narrow horizontal beam pattern, a broad vertical beam pattern, and a resonance frequency near 100 kHz. It became necessary to build a transducer, Projector A, for the experiment since numerous available transducers were found unacceptable. Figure 3.6 is an illustration of Projector A. The projector's active element was a solid block of a piezoelectric ceramic having the following dimensions: length - 3.4 cm; height - 1.91 cm; and thickness - 1.27 cm. The projector housing which held the element was made from a solid piece of plexiglass. A 0.375 in. hole was drilled in the top of the housing for inserting the projector's copper shaft. A smaller hole was bored from the interior backwall of the housing to the shaft hole which allowed the electrical leads access from the shaft to the element. Thin computer wire served as the electrical leads. Input and ground leads were drawn through the copper shaft and out the small hole bored in the housing's interior backwall. The element was polarized in the thickness mode with the ground lead soldered to the front active face while the input lead was soldered to the opposite face. At the other end, the leads were connected to a standard two-pronged electronic plug, which allowed rapid dismantling when the plug would not fit through auxiliary apparatus. The element was insulated on five sides with 0.125 in. thick neoprene and then slipped into its postion in the housing. The element was held securely in place by a small lip that extended from each of two plexiglass side-caps which were screwed into the housing. The projector housing was then dipped in liquid neoprene to seal it and allowed to dry for 12 hours. A 10 cm length of tape, graduated in millimeters, was placed on the shaft starting at the confluence of the shaft and

housing and extending up the shaft. The projector's depth was then read from the tape. The projector's resonance frequency was 88.2 khz with a strong harmonic at 161.5 khz. The projector's shaft, 0.375 in. by 51 in., was made excessively long to facilitate measuring the vertical directivity pattern. The horizontal and vertical directivity patterns will be discussed in section III-B-3.

4. Receivers and Receiver Assembly

Two LC-10 hydrophones were used as the receivers throughout the experiment. As mentioned earlier, Receiver A was located in Access A. It monitored the quality of the signal propagating in the fluid wedge and assisted in ensuring that the acoustic axis of the projector was properly aligned with the longitudinal centerline of the enclosure each time the projector was raised or lowered.

Receiver B was located in the tap water and secured by an aluminum assembly which was comprised of a securing block, containing the receiver, a sliding block located on the long arm, and a rod which connected the blocks. Although the sliding block could be moved along the entire length of the long arm, it remained fixed at distance of 20 cm from the fluid wedge enclosure. The rod was fixed in the securing block but was allowed to pass vertically through the sliding block by adjusting a thumb screw. Therefore, adjusting the rod raised or lowered the receiver. Millimeter graduated tape was placed on the rod and provided the means for measuring Receiver B's distance from the wedge apex. The initial position for Receiver B was in the water with its acoustic center directly beneath the apex of the fluid wedge in the vertical plane of the projector's acoustic axis. As the rod was lowered in the water, it remained parallel to the front sidewall while the receiver remained perpendicular to the rod and the frontwall. Figure 3.7 shows Receiver B and the receiver assembly.

5. Electronic Equipment Set-up

Figure 3.8 provides a block diagram of the equipment set-up. Figure 3.9 is a photograph of the equipment. The projector was driven by a Hewlett-Packard 3314A Function Generator. The settings were as follows: frequency - 88.2 kHz; amplitude - 6.0 v; and tone burst - 32 cycles. The digital function generator consclidated the functions of an oscillator, tone burst generatcr, and frequency counter in one unit. All system outputs were monitored readily by reading a digital display. Its flexibility proved useful when the tone burst had to be adjusted to assist in identifying and measuring the correct signal. The output signal from Receiver B was first patched through an Ithaco 1201 Low Noise Preamplifier and then on to channel A of the Nicolet Oscilloscope. The preamplifier settings were as follows: gain - 1k; highpass filter - 3k; and low pass filter - max. The preamplifier successfully suppressed 60 Hz noise and amplified the signal appropriately. The output signal from Receiver A was passed through a 60 Hz filter which was inserted into a Hewlett-Packard 465A Amplifier set at 40 dB gain and then on to channel B of the Nicolet Oscilloscope. The Nicolet displayed simultanecusly both output signals and allowed the presentations to be expanded and stopped. When required the output of the function generator was also monitored on the Nicolet. By aligning a horizontal cursor to the signal, the voltage amplitude was read from a digital read-out in the lower right hand corner of the display area. Time was obtained by adjusting a vertical cursor and reading a second digital read-out in the lower left hand ccrner of the display area. The Nicolet was synchronized externally by the function generator.

6. Auxiliary Apparatus

The following additional equipment was used during various aspects of the experiment:

a. Measuring the Speed of Sound:

(1) Plastic rectangular tub

(2) Aluminum stand assembly

b. Measuring the Densities of the Liquids:

(1) ASTM graduated cylinder

(2) Analytical balance with weights

c. Filling the Enclosure with Fluid:

(1) 1000 ml plastic pitcher

(2) Plastic funnel with Tygon tubing

d. Measuring the Level of the Enclosure and Pressurizing the Enclosure

(1) Plastic level

(2) Portable hand pump

C. PROCEDURE

Prior to commencing the actual data measuring events, the speeds of sound and the densities of the transducer fluid and tap water were measured. This was done to verify that the speed of sound of the transducer fluid was indeed slower than that of the tap water. Also, it was mandatory to calculate the speed of sound and density ratios as they were required variables in the computer model. Additionally, the horizontal and vertical far-field directivity patterns of Projector A were measured to verify the projector's usefulness for the experiment.

1. Sound Speed Measurements

The speeds of sound of the two liquids were measured using identical equipment set-ups. A plastic tub measuring 45 cm by 30 cm by 25 cm was filled with the appropriate

liquid to a depth of 20 cm. Projector A and two LC-10 hydrophones, Receivers A and B, served as the transmitting and receiving units respectively. Two aluminum vertical stands with an aluminum bar clamped between them were positioned so that the plastic tub was set between the stands and directly beneath the bar. The two receivers were clamped to the bar with a distance of 35.0 cm. between them and lowered into the liquid so that their acoustic centers were at a depth of 10 cm. The projector was clamped to the bar and placed 10 cm. ahead of Receiver A, lowered into the liquid, and aligned acoustically with the receivers. Therefore, the order from left to right in the tub was Projector A, Receiver A, then Receiver B. The projector was driven by the Hewlett-Packard 3314A Function Generator and transmitted a pulsed 100 kHz signal. The output leads of the receivers were patched to 60 Hz filters which were connected to Hewlett-Packard 465A Amplifiers set at 20 dB. The output of the amplifiers was fed into the appropriate channel of the Nicolet Oscilloscope.

The time for the signal to transit from Receiver A to Receiver B was measured. The speed of sound was then calculated by dividing the distance between the receivers by the measured time delay. The speeds of sound of the transducer fluid and the tap water were 1377.07 m/s and 1509.14 m/s respectively.

2. Density Measurements

The densities of the liquids were measured by initially weighing an empty ASTM 100 ml graduated cylinder on an analytical balance which was accurate to one-tenth mg. The cylinder was then filled with 100 ml of the liquid to be measured and then weighed on the analytical balance. The weight of the liquid was found by subtracting the weight of the empty cylinder from the weight of the full cylinder.

The density was derived by multiplying the weight of the liquid in grams by 1000 and then dividing the product by the 100 ml volume to obtain the density in kg/m. The calculated densities were 975.0 kg/m and 992.0 kg/m for the the transducer fluid and tap water respectively.

3. Directivity and Beamwidth Measurements

The projector's far-field horizontal directivity pattern had to be narrow enough to ensure that minimal sound energy was reflected off the aluminum sidewalls while its far-field vertical directivity pattern had to be wide enough to ensure nearly complete ensonification of the fluid surface and the Mylar membrane. The experimentally obtained directivity patterns compared favorably with theoretical expectations. Figures 3.10 and 3.11 illustrate the comparison between experimental and theoretical results for the horizontal and vertical far-field directivity patterns respectively. Figures 3.12 and 3.13 depict the directivity patterns within the enclosure for the horizontal and vertical patterns respectively.

The theoretical directivity for a rectangular piston is: [Ref. 6]

$$H(\theta,\phi) = \frac{\sin(1/2\ KL_1 \sin\theta)}{(1/2\ KL_1 \sin\theta)} \cdot \frac{\sin(1/2\ KL_2 \sin\phi)}{(1/2\ KL_2 \sin\phi)} \qquad \text{(eqn 3.1)}$$

Where:

L_1 = horizontal dimension of the active face

L_2 = vertical dimension of the active face

$K = w/c$ = Wave number

θ = horizontal angle measured from a major radiation axis

ϕ = vertical angle measured from a major radiaton axis

In this case when the horizontal directivity is desired, ϕ is set to zero. Conversely, when the vertical directivity is desired, θ is set to zero.

The horizontal directivity was measured in the fluid wedge enclosure. The enclosure was placed level (zero elevation angle) and filled with transducer fluid tc a depth of 8.0 cm. Receiver A was placed in Access A and lowered into the fluid so that its acoustic center was at 4 cm. below the fluid surface. The receiver output lead was connected to the Y-input of an X-Y plotter, a voltmeter, and channel B of the Nicclet oscillcscope. Projector A's shaft was placed through an electrical-mechanical device which when operated rotated the projector through 360 degrees. The device with the projector installed was then placed on the top of the fluid wedge enclosure over the Access C opening and the projector was lcwered into the fluid so that its acoustic axis was 4 cm below the surface and acoustically aligned with Receiver A. The output lead of the rotating device was connected to the X-input of the X-Y plotter. The output of the X-Y plotter produced a horizontal directivity.

As a matter of convenience, the vertical directivity was measured in the water tank with tap water as the medium. Again, Projector A and Receiver A were utilized as the transmitting and receiving units respectively. As indicated from equation 3-1, maintaining the same wavelength produces an identical directivity pattern. A frequency of 96.6 kHz in water with a speed of sound of 1509.14 m/s produced the same wavelength as a frequency of 88.2 kHz in transducer fluid with a speed of sound of 1377.07 m/s.

The equation for determining the beamwidth of the main lobe of the horizontal or vertical far-field directivity function is as follows: [Ref. 9]

$$\Delta\theta \text{ or } \Delta\phi = 2 \sin(x\, c / f\, L) \qquad \text{(eqn 3.2)}$$

where:

$\Delta\theta$ = horizontal beamwidth

$\Delta\phi$ = vertical beamwidth

c = speed of sound of the medium

f = frequency of the projector

L = the horizontal or vertical dimension of the piston

x = Factor derived for the desired main lobe decibel (dB) down point. (As an example for -3 dB, x = .443; for -6 dB, x = .603; and for -180 dB (null), x = 1)

Table I tabulates the results of the predicted and experimental beamwidths.

TABLE I

Beamwidth Comparisons

dB Down Point	Horizontal Beamwidth Theory	Horizontal Beamwidth Experimental	Vertical Beamwidth Theory	Vertical Beamwidth Experimental
-3	9.55	8.0	42.42	50.0
-6	12.97	11.6	59.00	60.0
-180	21.40	20.0	109.52	78.0

The inner boundary of the far-field of the projector was obtained from the following equation: [Ref. 9]

$$R = \frac{\pi f \{(L_1/2)^2 + (L_2/2)^2\}}{c} \qquad \text{(eqn 3.3)}$$

where:

L_1 = Horizontal dimension of the active face

L_2 = Vertical dimension of the active face

c = Speed of sound of the medium

f = Frequency of the projector

For Projector A, R equals 37.34 cm.

4. Fluid-Wedge Angle Measurements

It was originally intended to measure the fluid-wedge angle by reading the compass-rose attached to the sidewall of the wedge enclosure. The compass-rose readings proved too inconsistent to be used alone for obtaining the wedge angle. However, it did provide useful estimates of the wedge angle during the time that the enclosure was being prepared for each measuring event. As a result, the etched lines on the backwall of the enclosure in conjuction with the graduated measuring tape on the backwall were relied upon to furnish accurate fluid depth readings. The apex measurement was strictly a visual determination as to whether or not the fluid made contact with the most forward part of the Mylar at the interior side of the frontwall. Before each measurement the Mylar surface was inspected to ensure that no wrinkles or bowing was present.

5. Measurements of the Pressure Profile Beneath the Apex

Each measuring event followed a standard procedure for setting the fluid wedge angle and the depths of the projector and receivers.

The horizontal bar, that supported the long arm of the enclosure, was raised and clamped into position. The compass-rose was checked to verify that the enclosure had been elevated to form the desired fluid wedge within the enclosure. If not, the horizontal bar was adjusted until the wedge angle was reached. The level of the enclosure was checked using a plastic level mounted on the top of the

enclosure. When required, the set screws on the angle iron of the pivot arm were adjusted so that the enclosure was level in relationship to the water surface in the tank. Tap water was then added to the tank until the water just made contact with the Mylar at the interior edge of the enclosure's frontwall. Because of the density difference between the fluids, the addition of the water caused the Mylar to wrinkle and bow inward unless a compensating quantity of fluid was added to the enclosure.

Transducer fluid was poured slowly into the enclosure using a plastic 1000 ml pitcher in combination with a plastic funnel which had a short length of Tygon tubing attached to its outlet. The funnel was placed in Access B (fluid inlet port) with the tubing set along the sidewall submerged in the fluid. This procedure minimized the introduction of air bubbles into the fluid. Transducer fluid was added until the leading edge of the fluid wedge, advancing up the incline, reached the apex position at the frontwall and the fluid level at the backwall reached the proper depth. The liquid levels and wedge angle were adjusted as necessary until achieving the desired wedge angle and a flat "mirror-like" Mylar surface.

Receiver A was lowered into the fluid until its acoustic axis was midway between the Mylar and fluid surface. Receiver B was positioned in the tap water with the acoustic center directly beneath the apex of the fluid wedge on the center line of the frontwall. Projector A was positioned in the fluid wedge with its acoustic axis at a depth equal to either one-half or one-quarter the wedge angle. (Readings were taken with the projector at both depths.) While the outputs of the receivers were being monitored, the projector was aligned so that its acoustic axis coincided with the longitudinal centerline of the enclosure, and then locked in position. Receiver A was then

retracted from the fluid to eliminate possible interference or reflections caused by its presence.

Voltage amplitude readings were then ready to be taken and recorded. Figure 3.9 provides a block diagram of the equipment set-up. Receiver B was lowered in the tap water directly beneath the apex in the vertical plane of the projector's acoustic axis until the maximum voltage amplitude was located and recorded. The receiver was then returned to the start point where the initial readings for the measuring event were taken. As Receiver B was lowered in the water, depth and voltage data were taken in 0.5 cm increments until a depth was reached which corresponded to a nondimensional depth (z/X) of approximately 3.0. The number of data points required ranged from a high of 74 for a two degree wedge angle to a minimum of 32 for a ten degree wedge angle.

Measurements taken at four, six, and eight degrees were taken with the enclosure pressurized as well. The procedure was the same as described above except that a small amount of fluid (approximately 0.1 cm according to the backwall tape) was added to the enclosure to compensate for the downward force which subsequently would be exerted upon the fluid by pressurizing the enclosure. The enclosure was made airtight by sealing all access ports securely and tightening the fittings that held the shafts of Projector A and Receiver A. Once airtight, the air hand pump was attached to the air control valve and the enclosure pressurized. Pressure was admitted until the leading edge of the fluid receded from the frontwall of the enclosure and the fluid level dropped below the desired depth. The pump was then disconnected and air was bled from the enclosure until the leading edge of the fluid just touched the frontwall and the depth of the fluid was at the desired level. Again, the surface of the Mylar was inspected to ensure that it was

flat and "mirror-like." The difference in densities was 17 kg/m, thus minimal pressure, approximately 0.04 ounces per square inch, was required to equalize the forces on the Mylar membrane. When the projector had to be repositioned for the second reading of an event, the enclosure was repressurized and the wedge stabilized as before.

Data were taken from the Nicolet oscilloscope by visual integration. Generally, reflections were well separated from the signal. However, when reflections did overlap the signal, the surface of the water was agitated, thus revealing the reflected signal. When Receiver B was approaching a minimum in the pressure profile, the signal became quite distorted which degraded the ability to visually integrate the signal. Conversely, during periods when the amplitude was increasing or at a maximum the signal was well formed and produced acceptable data. During the final measuring event, the projector was moved forward to Access B to determine whether or not projector location affected the pressure profile. The signal received during that event was superior to all other signals obtained in previous events. Regardless of the pressure profile, the signal was sharp and exceptionally well formed and posed no visual integration difficulties.

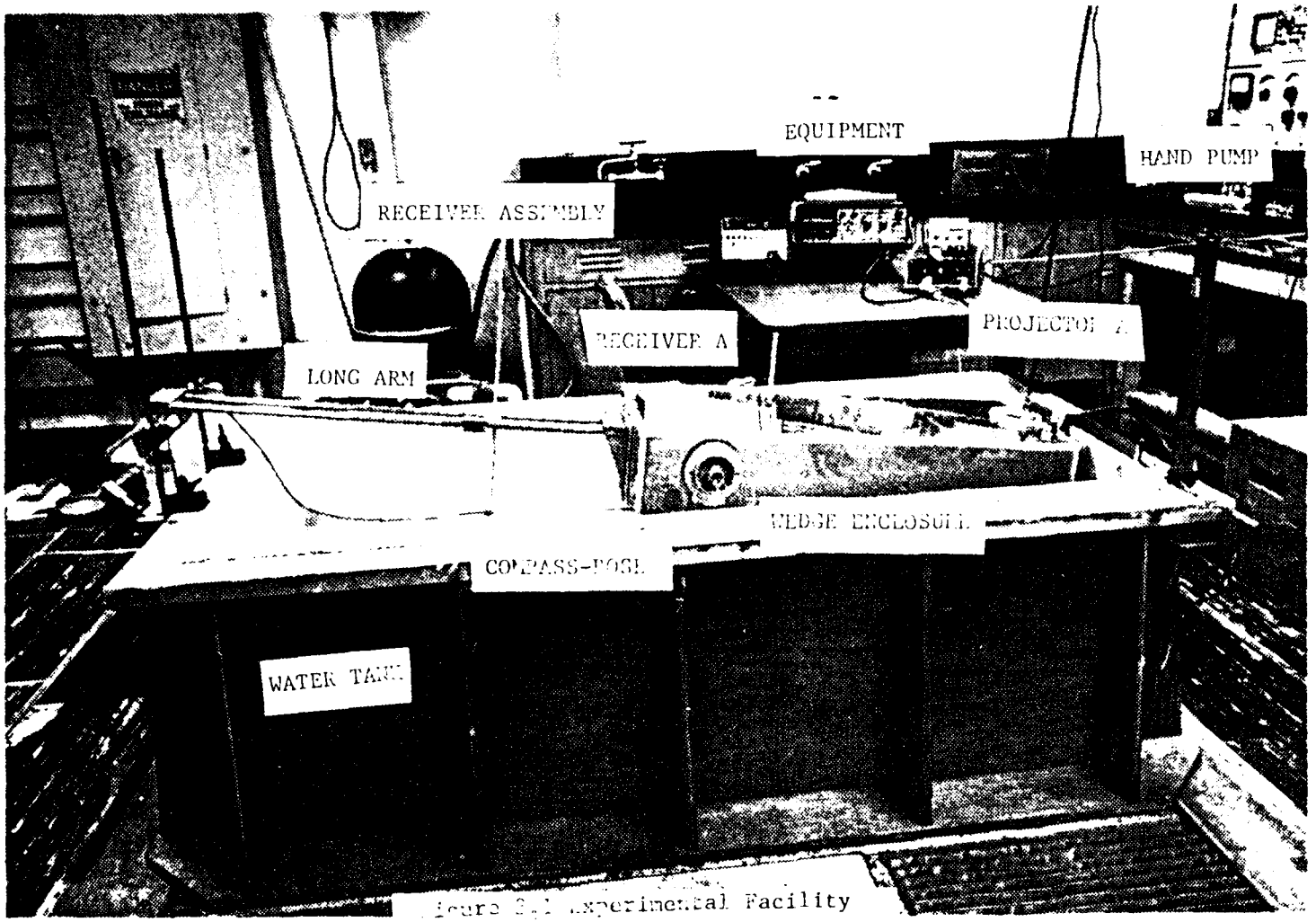

Figure 3-1 Experimental Facility

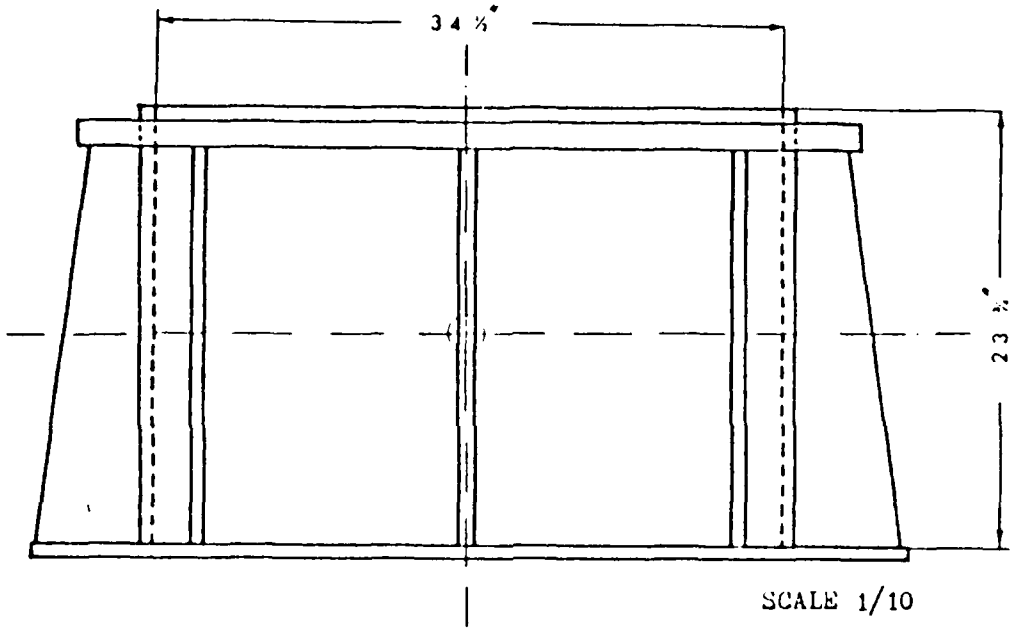

Figure 3.2 Water Tank (side view)

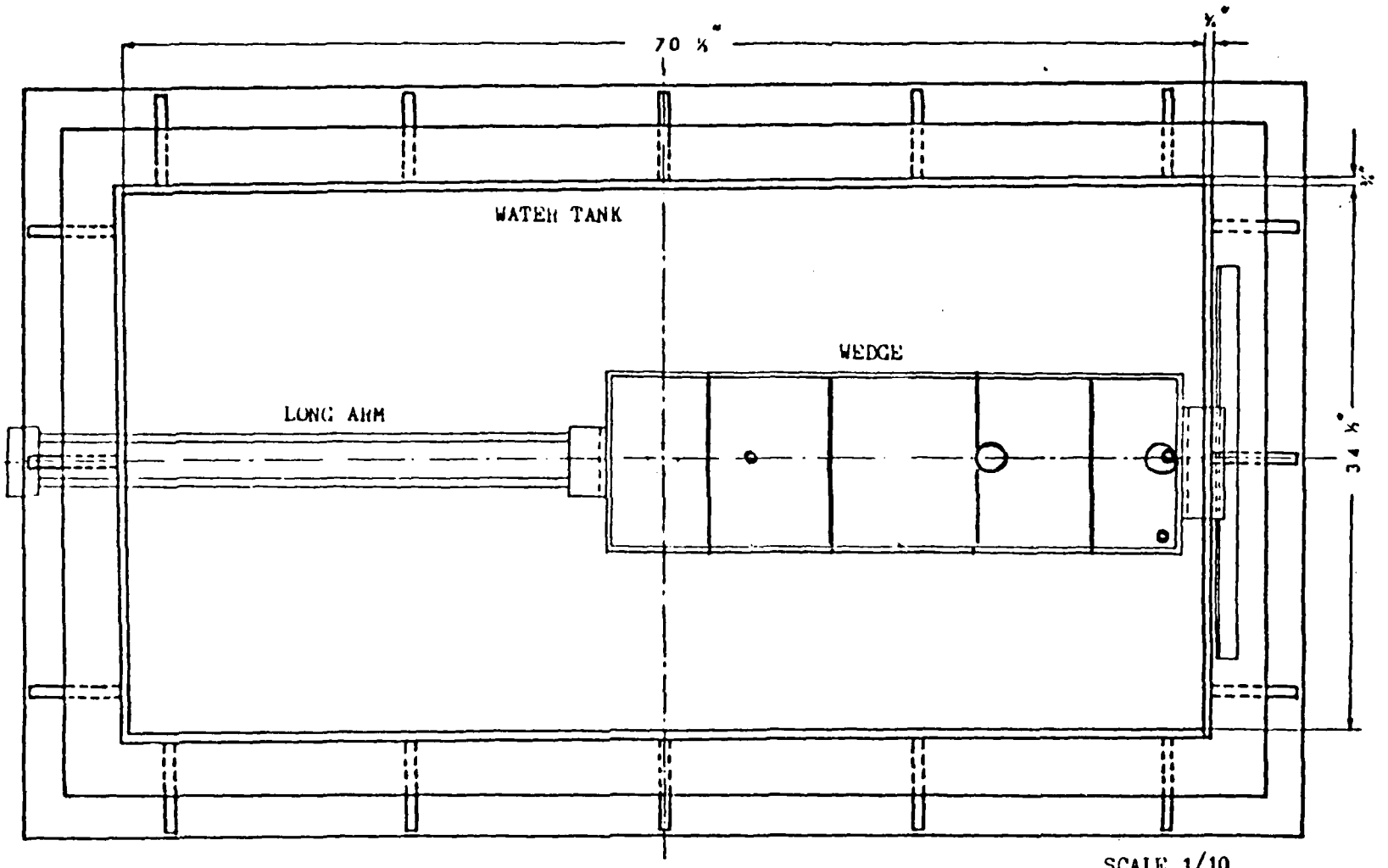

Figure 3.3 Water Tank and Enclosure

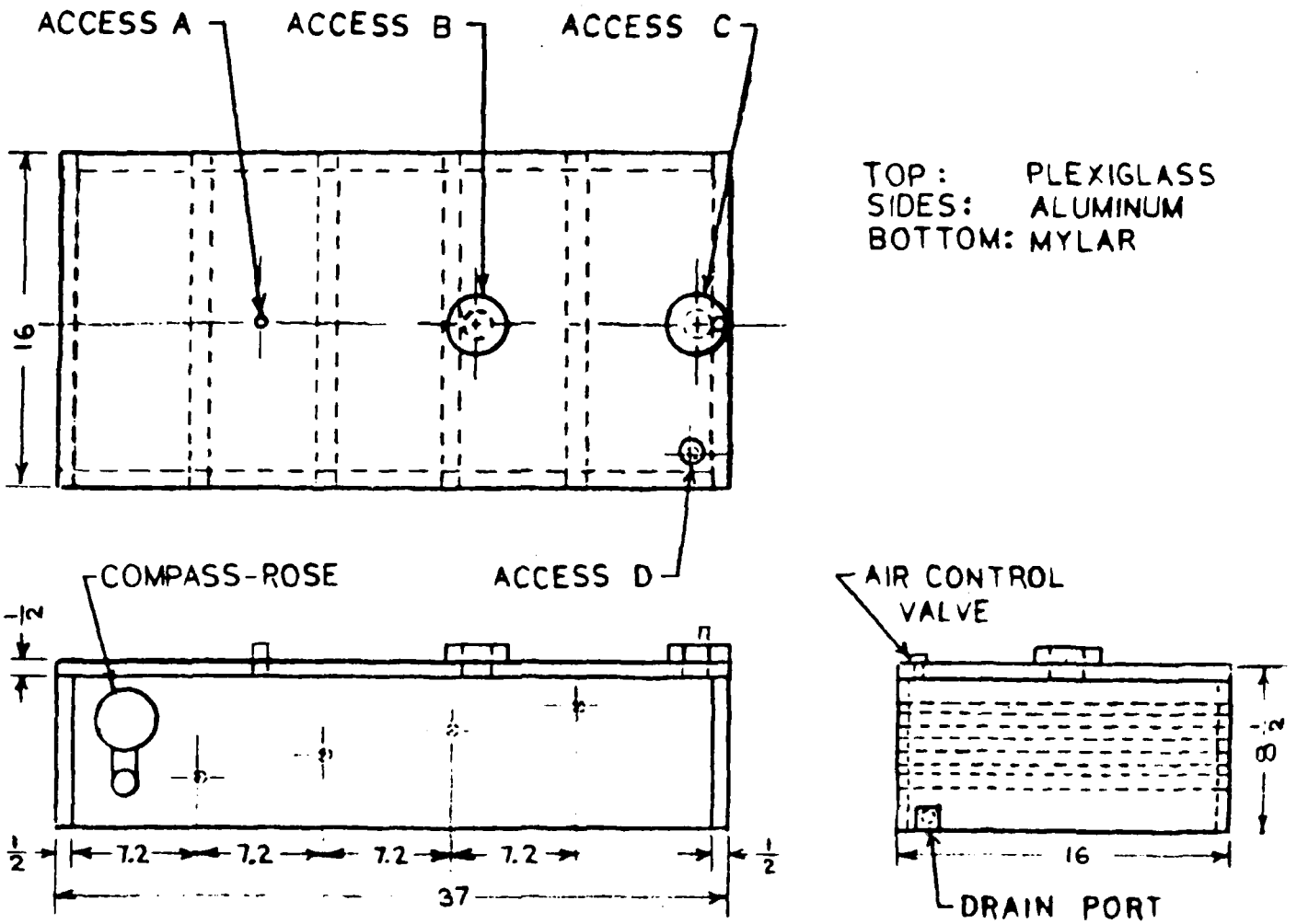

Figure 3.4 Wedge Enclosure

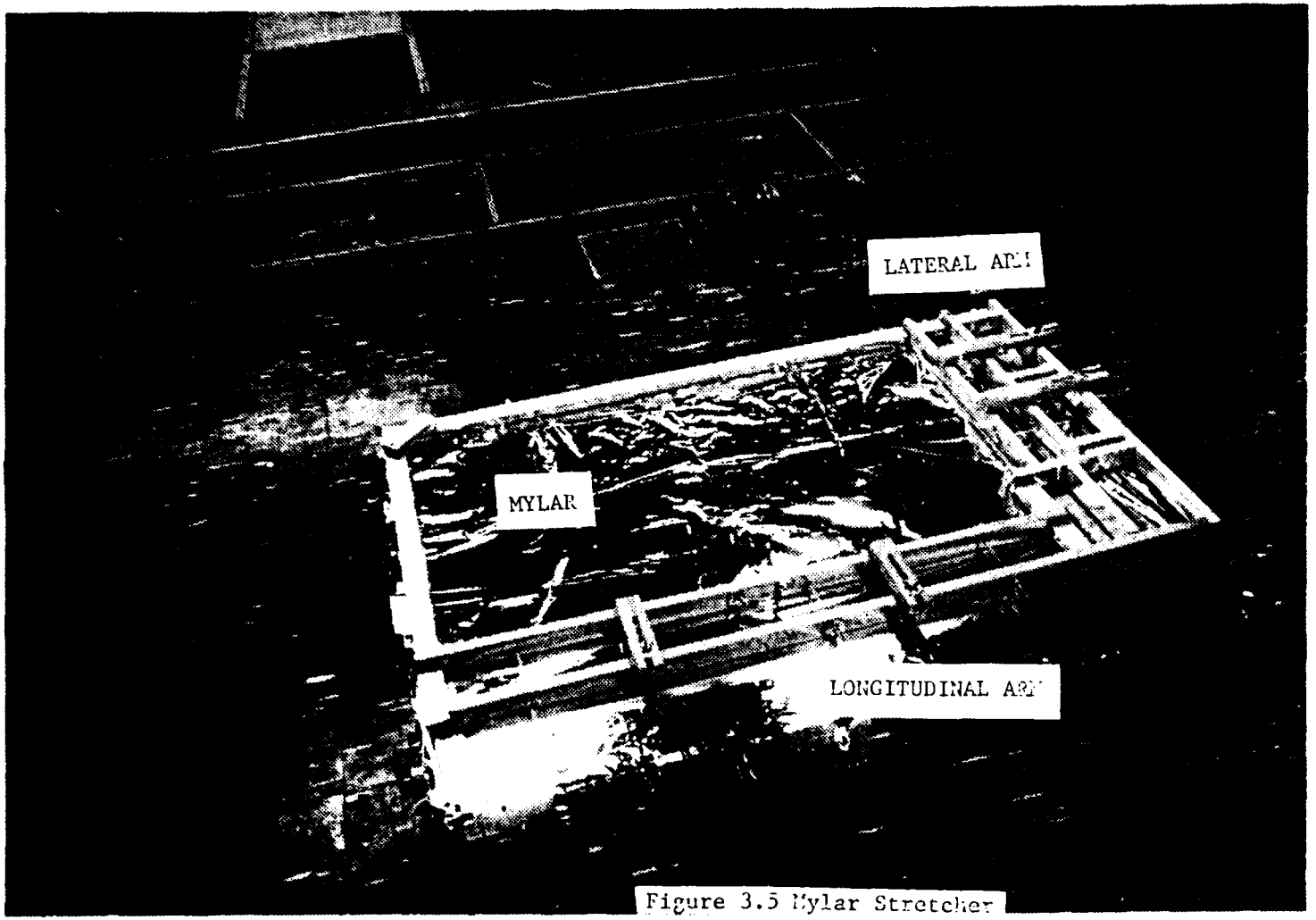

Figure 3.5 Mylar Stretcher

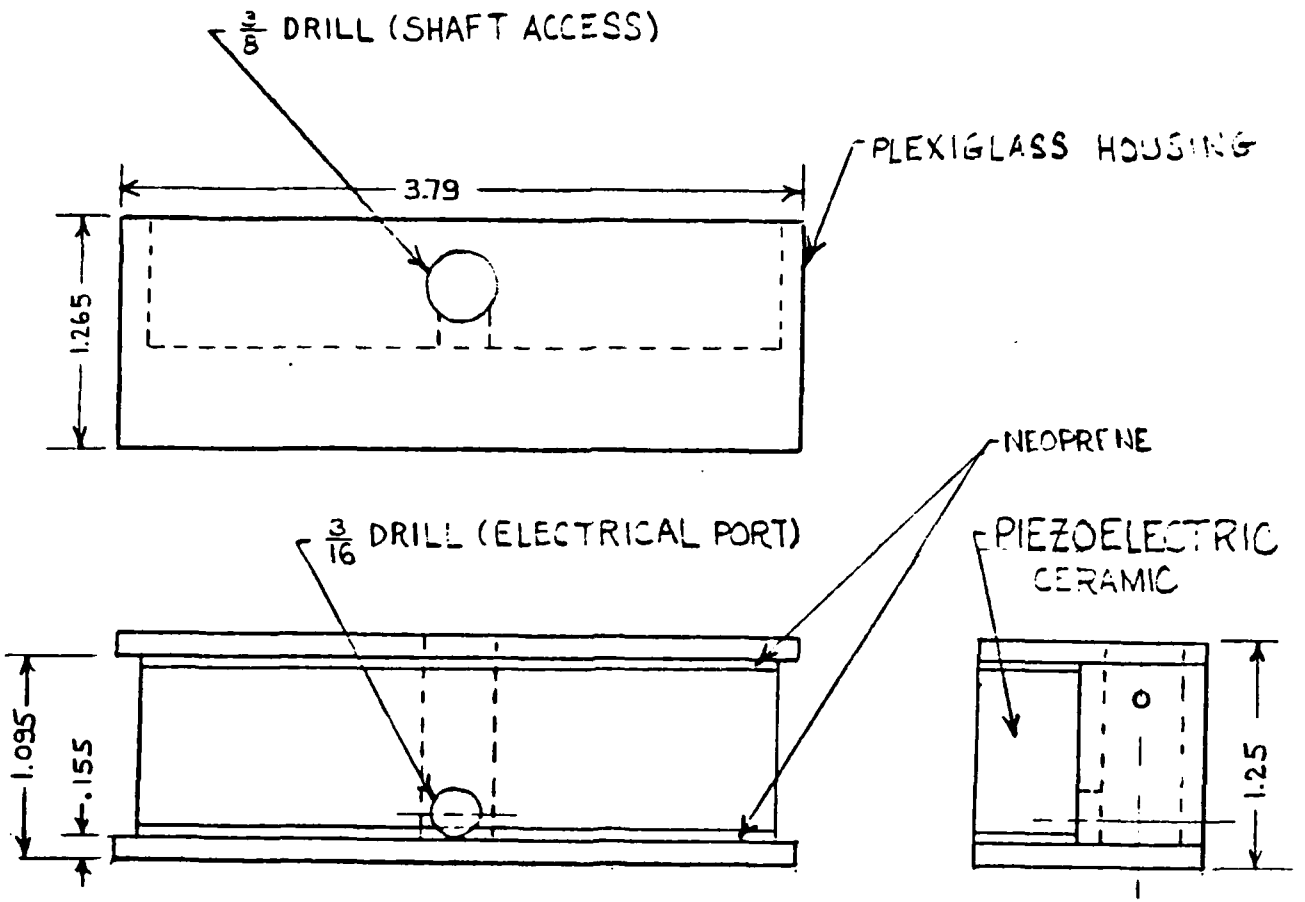

Figure 3.6 Projector A

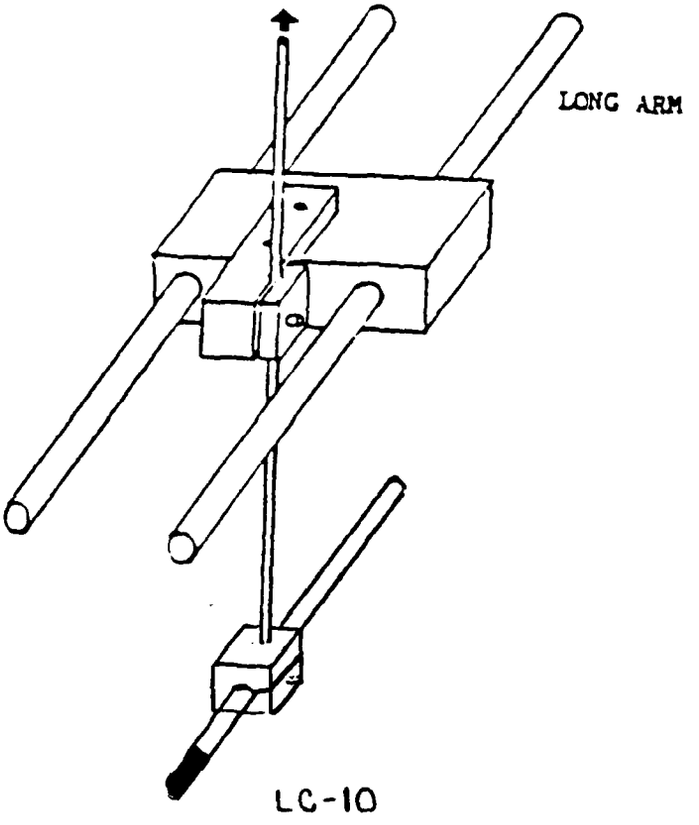

Figure 3.7 Receiver B and Assembly

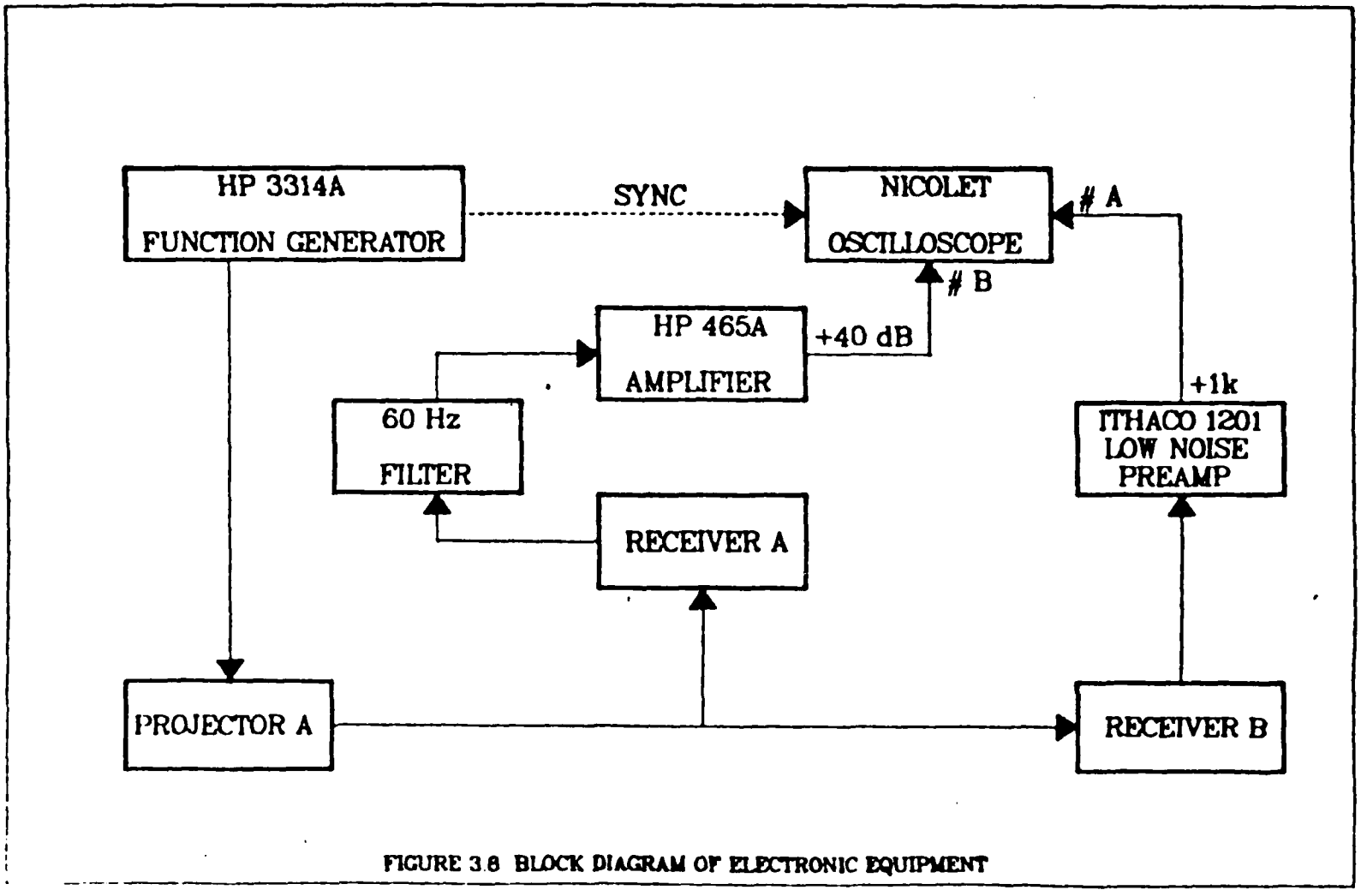

FIGURE 3.8 BLOCK DIAGRAM OF ELECTRONIC EQUIPMENT

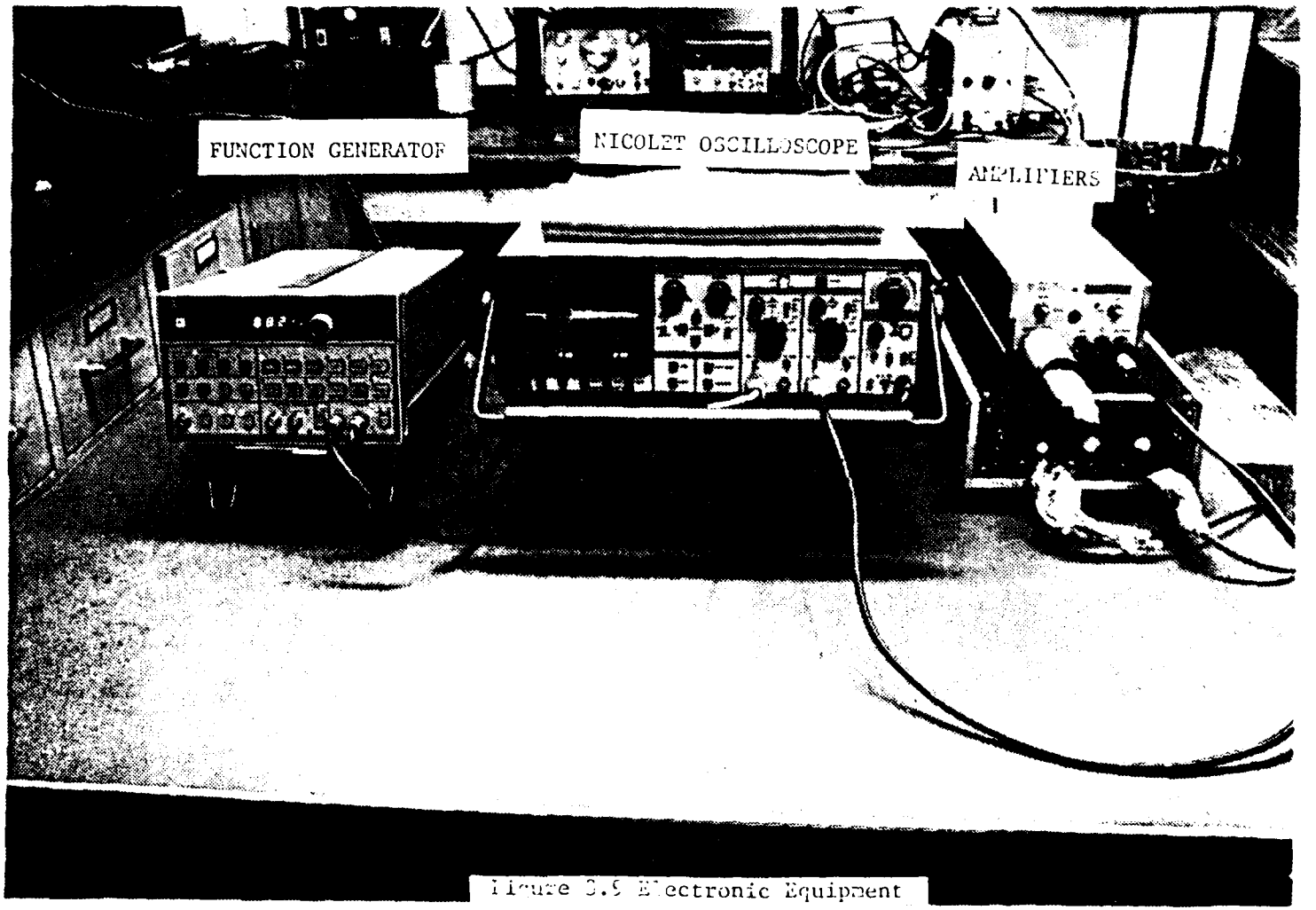

Figure 3.9 Electronic Equipment

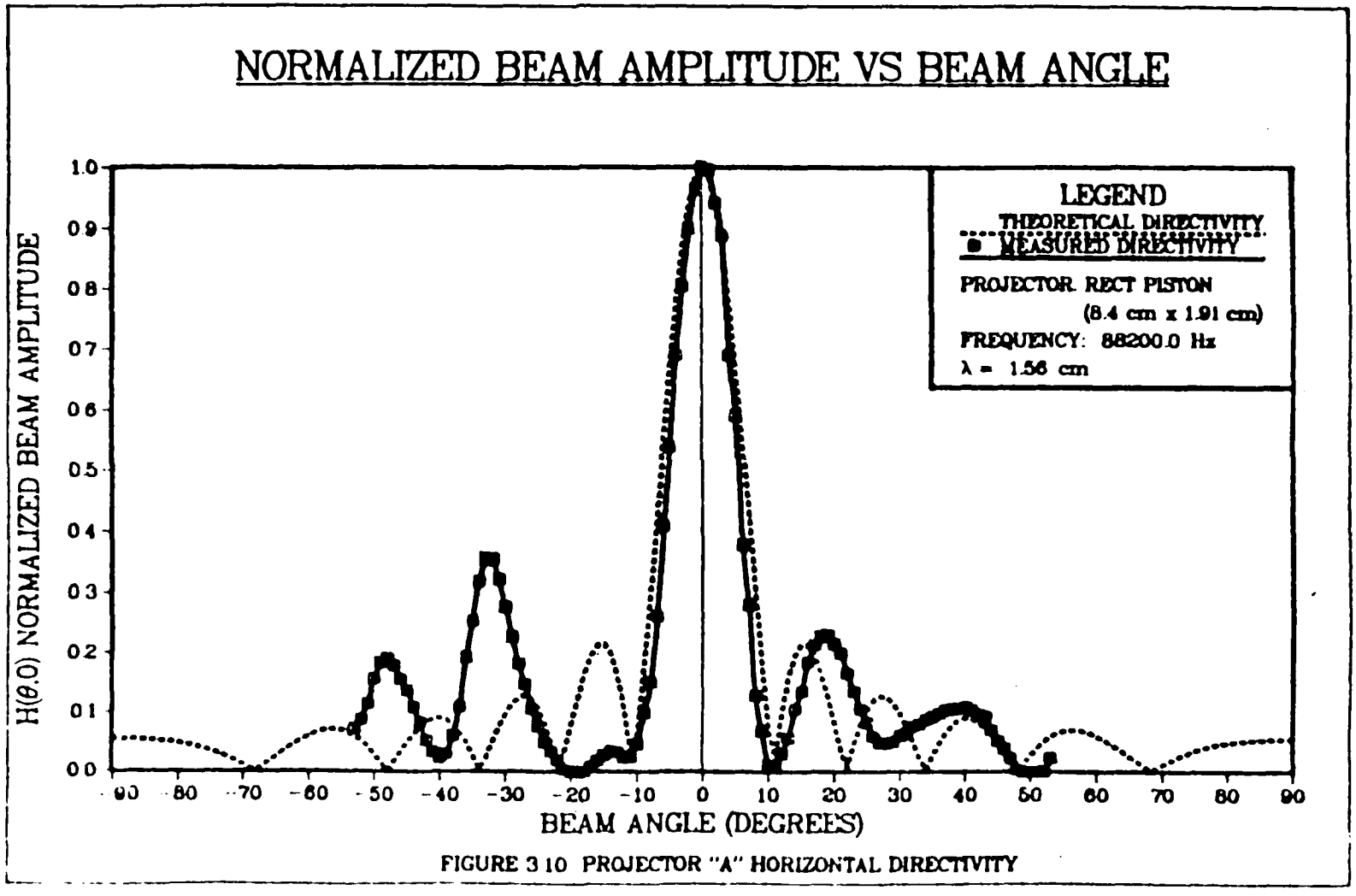

FIGURE 3.10 PROJECTOR "A" HORIZONTAL DIRECTIVITY

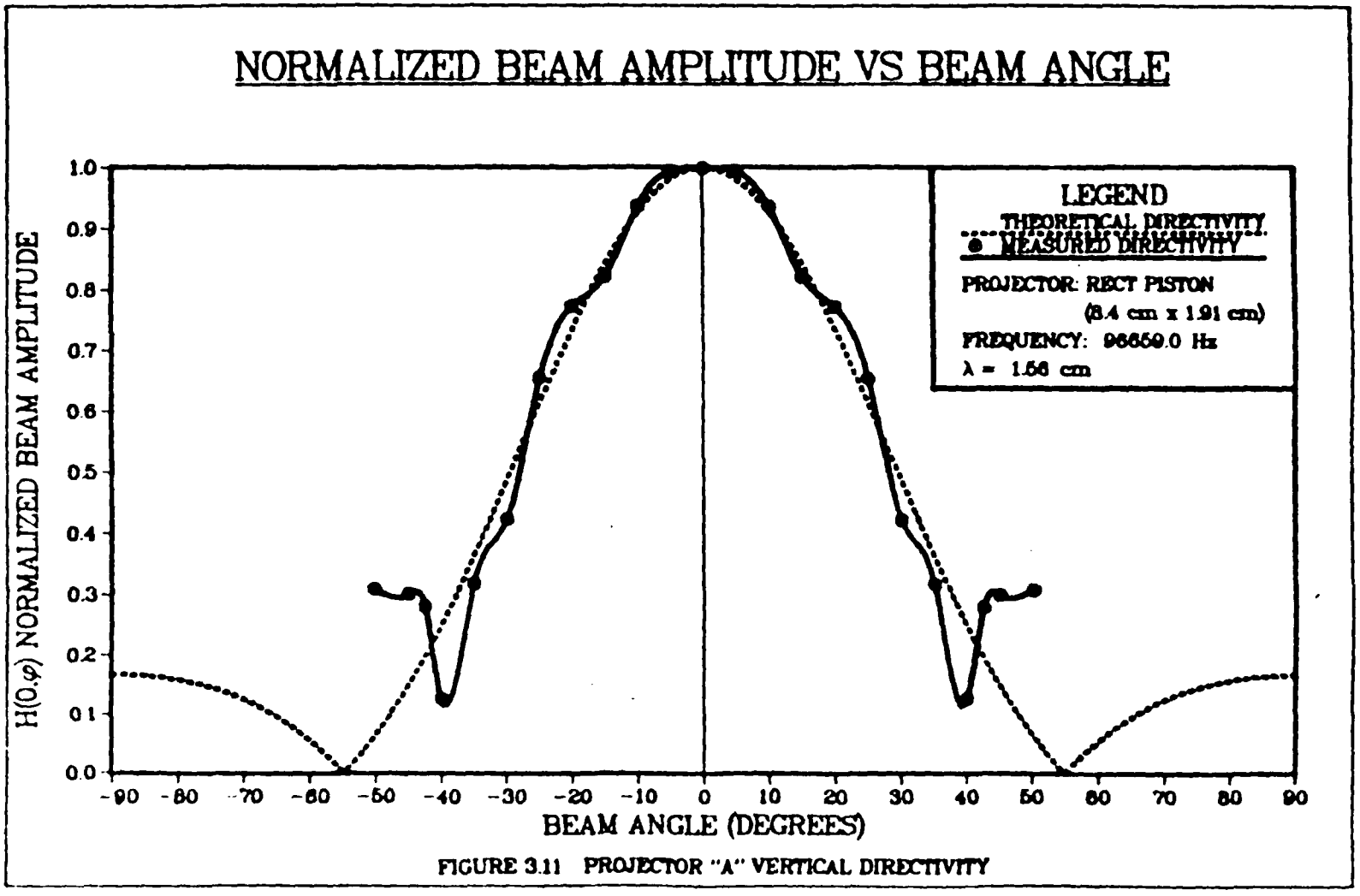

FIGURE 3.11 PROJECTOR "A" VERTICAL DIRECTIVITY

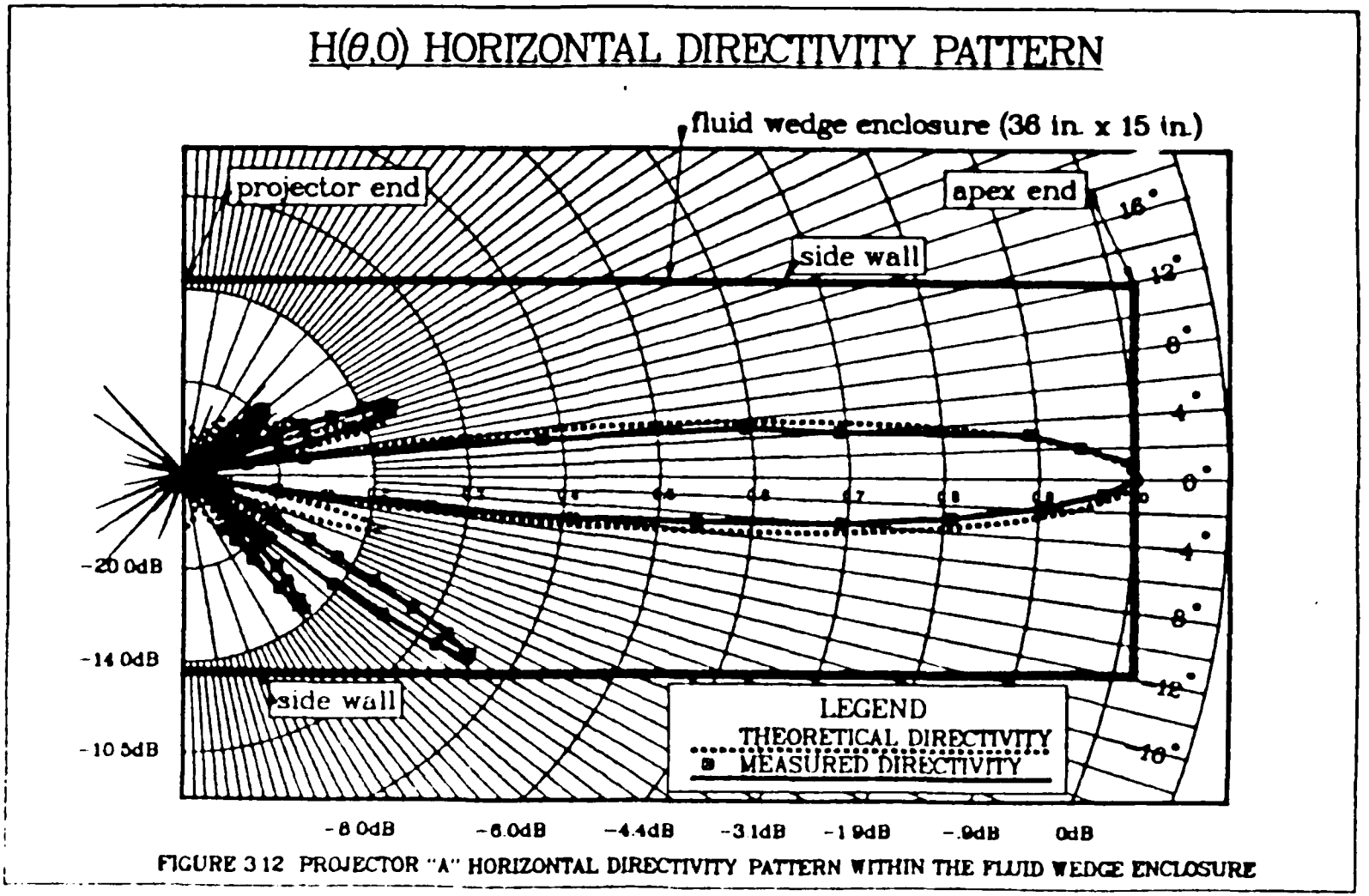

FIGURE 3.12 PROJECTOR "A" HORIZONTAL DIRECTIVITY PATTERN WITHIN THE FLUID WEDGE ENCLOSURE

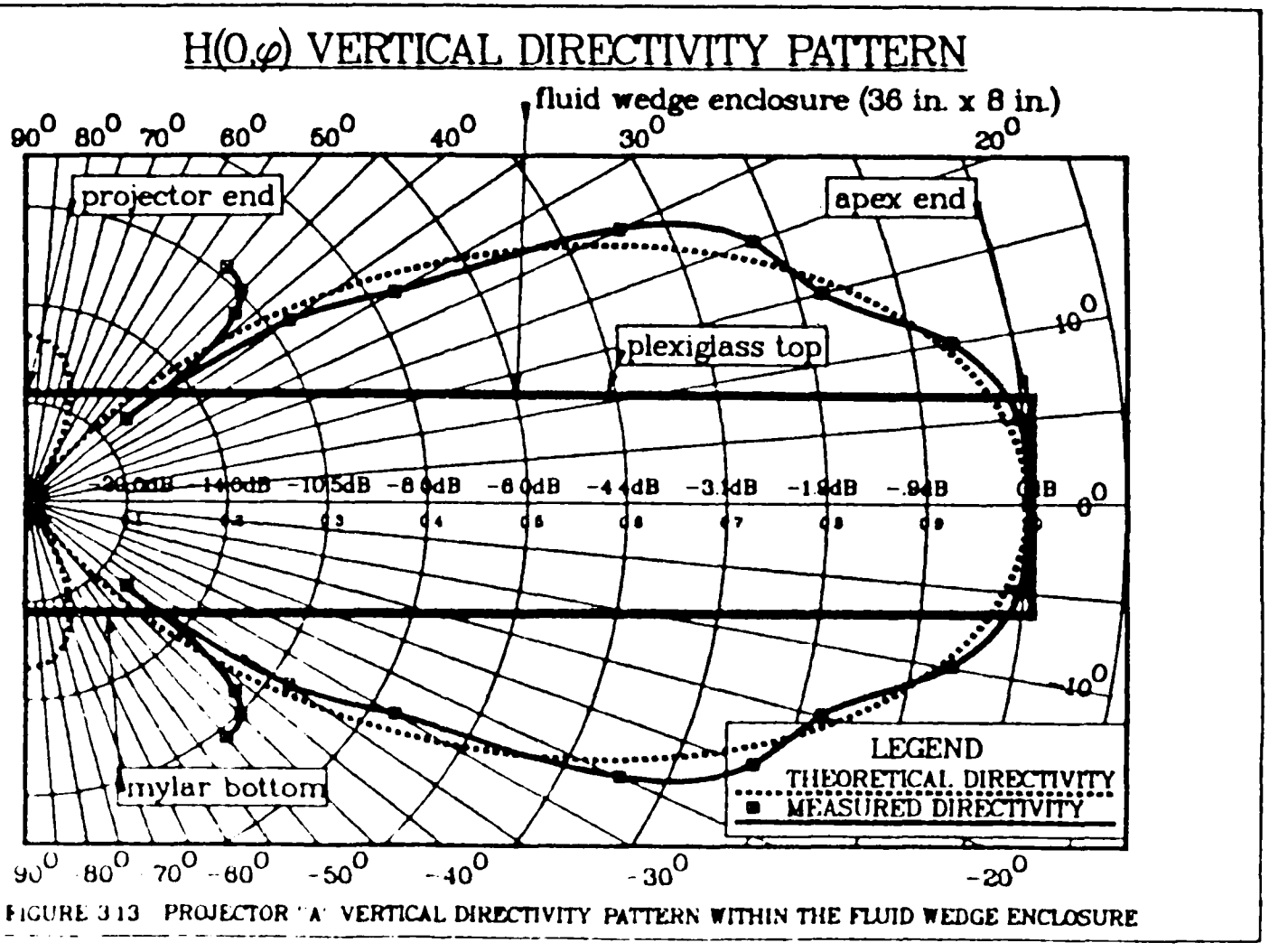

FIGURE 3.13 PROJECTOR 'A' VERTICAL DIRECTIVITY PATTERN WITHIN THE FLUID WEDGE ENCLOSURE

IV. RESULTS

The results of the experiment are best presented in four phases, which relate to the objectives listed in the Introduction. Phase I will compare the experimental results of a nonpressurized enclosure tc the theoretically predicted results. Phase II will compare pressurized results to theoretical and nonpressurized results for similar acoustical and geometrical parameters. Phase III presents comparison of the depths of maximum pressure as functions of wedge angle fcr nonpressurized and theoretical data for two projector elevation angles. Phase IV will discuss the data obtained when the prcjector was repositioned closer to the apex. For Phases I, II, and IV, the figures display the normalized pressure amplitude as a function of nondimensional depth, z/X, where z is the depth of Receiver B below the apex and X is the dump distance. The figures illustrating Phase IV plot the nondimensional depth of the first maximum pressure as a function of wedge angle for each of the two projector elevation angles. In addition to identifying the curves being compared, the figures list the appropriate acoustical and geometrical parameters.

A. PHASE I - EXPERIMENTAL AMPLITUDES VERSUS THEORETICAL PREDICTIONS

Figures 4.1 through 4.9 compare measured and theoretical pressure amplitudes as a function of depth for five wedge angles (β): 2.22, 4.12, 6.0, 8.0, and 10.0 degrees. Each plot represents one wedge angle and one of two projector elevation angles (δ), either one-half or one-quarter the wedge angle. With the exception of the 2.22 degree wedge

angle, all wedge angles were plotted twice. The vertical dimension of the projector's active face prevented its acoustic center from being lower than 1.03 degrees from the Mylar membrane, thus the projector could not be lowered to the one-quarter elevation angle of the first wedge angle.

Figure 4.1 (β = 2.22, γ = 1.11) indicates a most favorable comparison. The depth at which the maximum pressure occurs coincides while the remainder of the profile parallels the predictions with only a slight off-set. The data indicates a larger second maximum than expected, but the third maximum is of the same amplitude as predicted, although observed slightly farther from the apex. The two minima, immediately following the maximum pressure, occur at the predicted depth, but at greater amplitudes.

Figure 4.2 (β = 4.12, γ = 2.06) shows agreement for the depth of maximum pressure and subsequent first minimum. Additionally, agreement is found in the depth region from 1.6 to 2.8, though displaced slightly. On first glance, the center region, 0.6 to 1.6, appears to show no correlation with theory and too much structure. However, closer inspection reveals that if the peaks of the three maxima in this region were connected and all points leading to and departing from the minima were disregarded the resulting curve would parallel the contour of the predicted curve. Clearly, phase interference was responsible for the observed structure in the region as the minima were distinguishable points on the oscilloscope. This would indicate that, perhaps, the interference was caused by some undetected physical aspect of the experimental facility.

Figure 4.3 (β = 4.12, γ = 1.03) is an excellent example of the predicted profile peaking at a pressure maximum and then experiencing a succession of minima and maxima. The measured maximum pressure coincides with theory, while the remaining profile mirrors the successive minima and maxima.

In each instance the maxima were of less amplitude, but the similarity of the profiles is obvious.

Figure 4.4 (β = 6.0, γ = 3.0) indicates the experimental data in the central region, 1.0 to 1.75, compares favorably with theory while in the shallower and deeper depths the profile is similar, but shifted in opposite directions. The depth of maximum pressure plots significantly deeper than predicted.

Figure 4.5 (β = 6.0, γ = 1.5) presents excellent correlation with theory. The pressure maxima and minima are of similar amplitude and the experimental curve has only minor lateral displacement.

Figure 4.6 (β = 8.0, γ = 4.0) reveals the first true indication of a possible breakdown in the theory. There is a vague similarity between the curves in the upper half of the profile (left half of the figure). The lower half of the profile (right half of the figure) produces no apparent correlation between curves. Unlike the predicted curve, the measured profile experiences a rapid succession of minima and maxima.

Figure 4.7 (β = 8.0, γ = 2.0) depicts better correlation between curves. The maximum pressure is closer to the predicted depth. Although the latter half of the figure provides minimal correlation, at more shallow depths the profile has much more structure than expected.

At this juncture an assessment of the previous data was in order. A thorough inspection of the physical apparatus was conducted to determine if the equipment had been correctly positioned. Initially it was thought that the rubber cones, set in the bottom of the tank, were causing an interference pattern so they were removed. Additionally, the projector's active face and the bottom of the mylar membrane (water side) were brushed off to remove any bubbles which might have formed on their surfaces, although none

were visible . All indications were that the geometrical parameters and equipment were set properly. Nevertheless, fluid was extracted from the enclosure and the wedge angle process repeated in preparation for retaking the eight degree wedge angle data. Unfortunately, the results were similar to those obtained previously.

Because of obtaining relatively poor correlation at wedge angles from eight to nine degrees, the prospects of the theory being applicable at such large angles appeared bleak. Yet, as indicated in Figure 4.8 (β = 10.0, γ = 5.0), the measured data provided one of the best correlations of the experiment. At shallow depths the data mirrored the predicted curve while at other depths it paralleled the predictions nicely.

Figure 4.9 (β = 10.0, γ = 2.5) reveals little apparent correlation, although at the shallow end of the figure the experimental curve proceeds along a route similar to the predicted curve, but at much reduced amplitude. At the predicted depth of maximum pressure, the experimental data plunges to its minimum value, but is immediately followed by a curve rising rapidly to its maximum. Once again inspecting the measured curve from an optimistic vantage point, had the minimum not been as severe the experimental results would have likely paralleled the contour of the predicted curve for almost the entire nondimensional depth, albeit at a much reduced amplitude.

B. PHASE II - COMPARISON OF PRESSURIZED AND NONPRESSURIZED RESULTS

The enclosure was pressurized and data measurements for two projector depths at each wedge angle were taken. Projector angles were as follows: 2.06 and 1.03 , 3.0 and 1.5, and 4.0 and 2.5 degrees at wedge angles of 4.12, 6.0,

and 8.0 degrees respectively. Figure 4.10 through 4.15 provide individual comparisons between experimental data under pressure and theoretical predictions. Figures 4.16 through 4.22 compare pressurized and nonpressurized experimental data.

Figure 4.10 (β = 4.12, δ = 2.06) shows that experimental data correlates well with the maximum pressure, however, the remaining profile only vaguely resembles the predicted curve. Again, if a line were drawn to connect the peaks of the three maxima immediately following the maximum pressure, a case could be made for an exceptional agreement between the two pressure profiles, except at a depth of 2.5 where the curves diverge.

Figure 4.11 (β = 4.12, δ = 1.03) reveals excellent correlation with the depth of maximum pressure. Subsequent minima and maxima are present but at significantly lower amplitudes than predicted. After a depth of 1.15 the experimental curve ceases to resemble the predicted curve.

Figure 4.12 (β = 6.0, δ = 3.0) indicates that the data parallels the predictions, particularly in the latter half of the figure. The maximum pressure is in the vicinity of that predicted, however, much greater detailed structure preceeds and follows the experimental maximum pressure.

Figure 4.13 (β = 6.0, δ = 1.5) provides good correlation between theory and experimental data, especially in the depth region, 0.5 to 1.7, which includes the maximum pressure depth. The region of 1.7 to 2.5 resembles theory but the alignment is skewed towards shallower depths.

Figure 4.14 (β = 8.0, δ = 4.0) shows a vague resemblance to theory in the shallow half of the figure. The depth of the maximum pressure occurs at 1.25 near the position where theory predicts the location of the second pressure maximum. A maximum does ccincide with the depth of the predicted maximum pressure, however, it is only 56 percent

of the amplitude of its counterpart. Data recorded from greater depths bore nc resemblance to theory.

Figure 4.15 (β = 8.0, γ = 2.0) shows general agreement between the two curves, but the measured data demonstrated more structure, particularly in the regions on either side of the maximum pressure. The maximum pressure depth is in agreement with theory.

Generally, pressurized and nonpressurized data were in agreement with one another as was expected and can be viewed in Figures 4.16 through 4.21. However, it was anticipated that the pressurized data would correlate better with the theoretical predictions, but this did not prove to be the case. A possible reason for this is that no precise measurement cf the pressure could be made with the experimental facility. It was thought that visual determinations of the pressure would be adequate in view of the minute pressure required. It is possible that the enclosure may have been overpressurized. Thus, the Mylar would tend to bow into the water disrupting the geometry cf the fluid wedge. It was noted that when the enclosure was purposely overpressurized the observed voltage amplitude decreased.

C. PHASE III - DEPTH OF FIRST MAXIMUM PRESSURE VERSUS WEDGE ANGLE

Figures 4.22 and 4.23 present graphical summaries of the comparison between theory and nonpressurized data depicting depths of the first maximum pressure as a function of wedge angle. Figure 4.22 is for the projector angle elevation at one-half the wedge angle. As can be seen from the figure, theory predicts a rather flat curve which oscillates between nondimensional depths of 0.27 tc 0.4. The measured results provide favorable agreement through the range of wedge angles.

Figure 4.23 is the summary for the projector elevation angle at one quarter the wedge angle. The predicted curve is generally flat with an increasing slope. One small maximum is located at a nondimensional depth of 0.63. The experimental data increases in slope as the wedge angle increases. The slope is greater than predicted and the appearance of the curve indicates greater fluctuations. Despite these facts, the experimental data is considered in agreement with theory.

D. PHASE IV - IMPACT OF PROJECTOR LOCATION ON THE PRESSURE PROFILE

Figure 4.24 (β = 10.0, γ = 5.0) shows the experimental results when the projector was relocated from Access C to Access B. The new location placed the projector at a distance 57.0 cm from the wedge apex but still in the far-field. As indicated, the curves do not correlate, except that the maximum pressure depths are in the vicinity of one another. Differences in the curves are not surprising since the computer model was designed for sources at infinite distance and small wedge angles. This particular data event is a worst case scenario as the projector is closer to the apex, thus the far-field boundary, and has a large wedge angle of ten degrees. The above not withstanding, relocating the projector closer to the apex reduces the number of dump points. A reduction of dump points equates to a reduction in the number of beams transferred into the substrate to interact and cause phase interferences. The signals received during the data event were exceptionally well formed throughout the entire nondimensional depth. The generally smooth curve in Figure 4.24 attests to that fact.

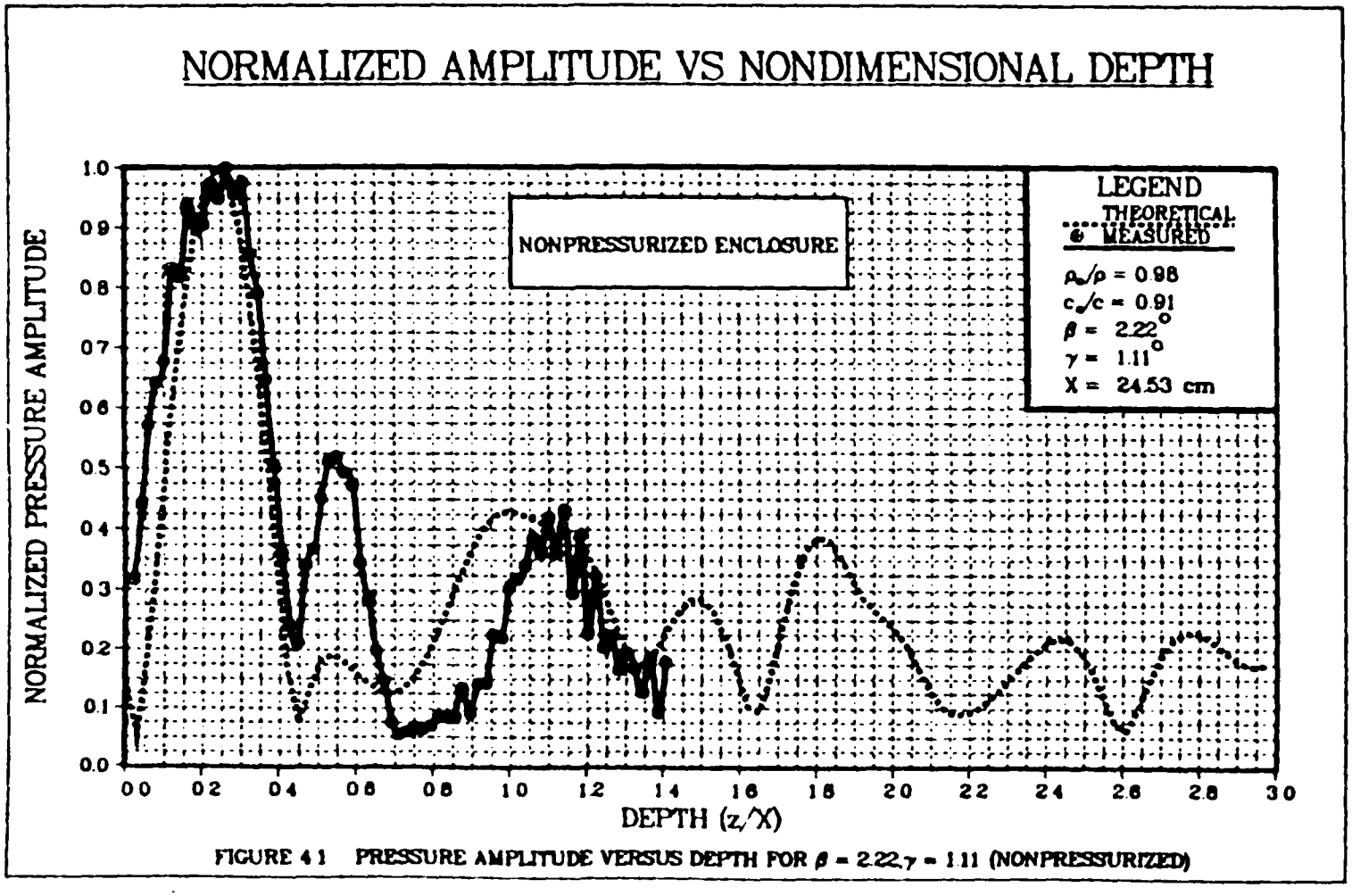

FIGURE 4.1 PRESSURE AMPLITUDE VERSUS DEPTH FOR β = 2.22, γ = 1.11 (NONPRESSURIZED)

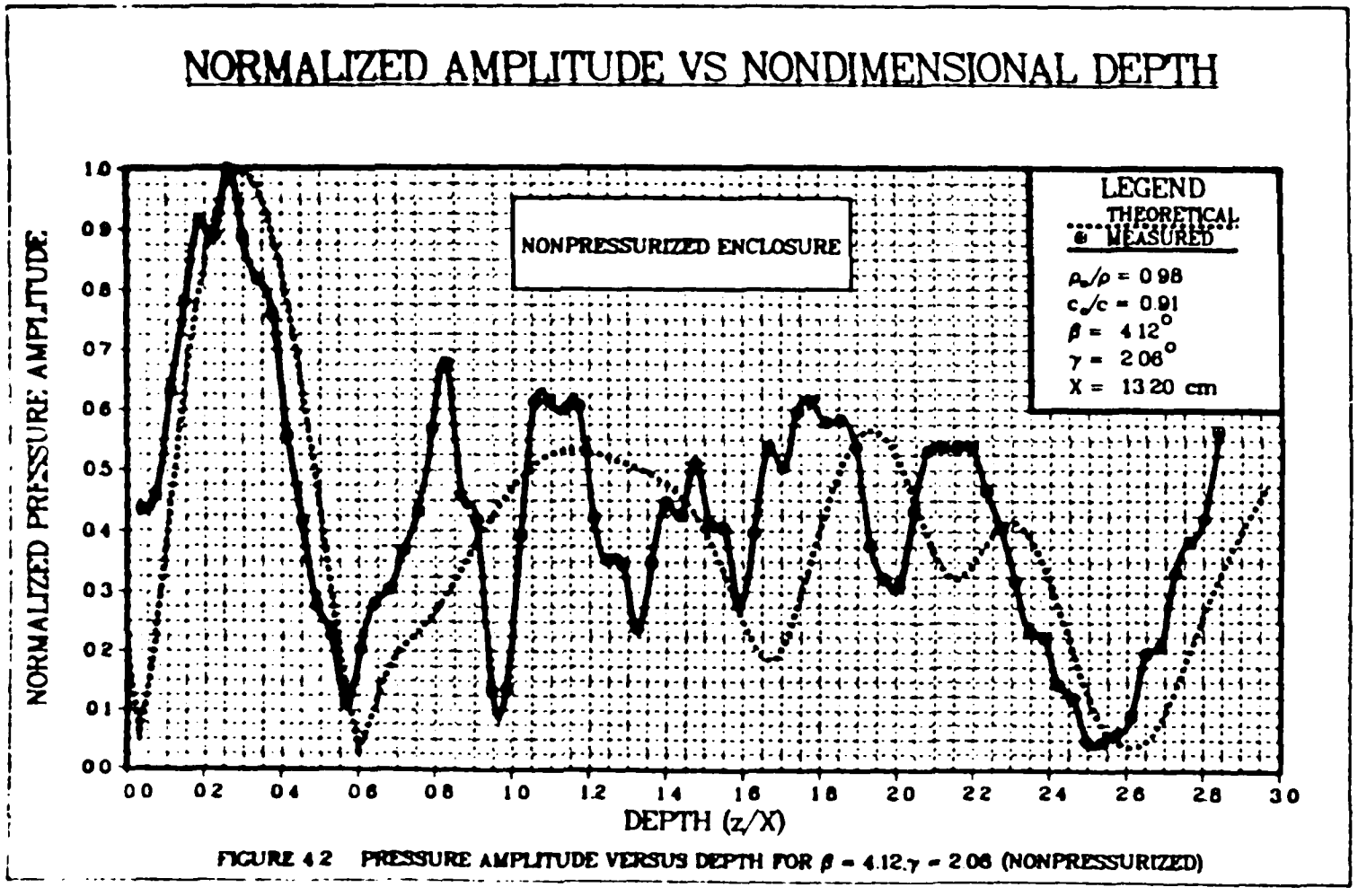

FIGURE 4.2 PRESSURE AMPLITUDE VERSUS DEPTH FOR β = 4.12, γ = 2.06 (NONPRESSURIZED)

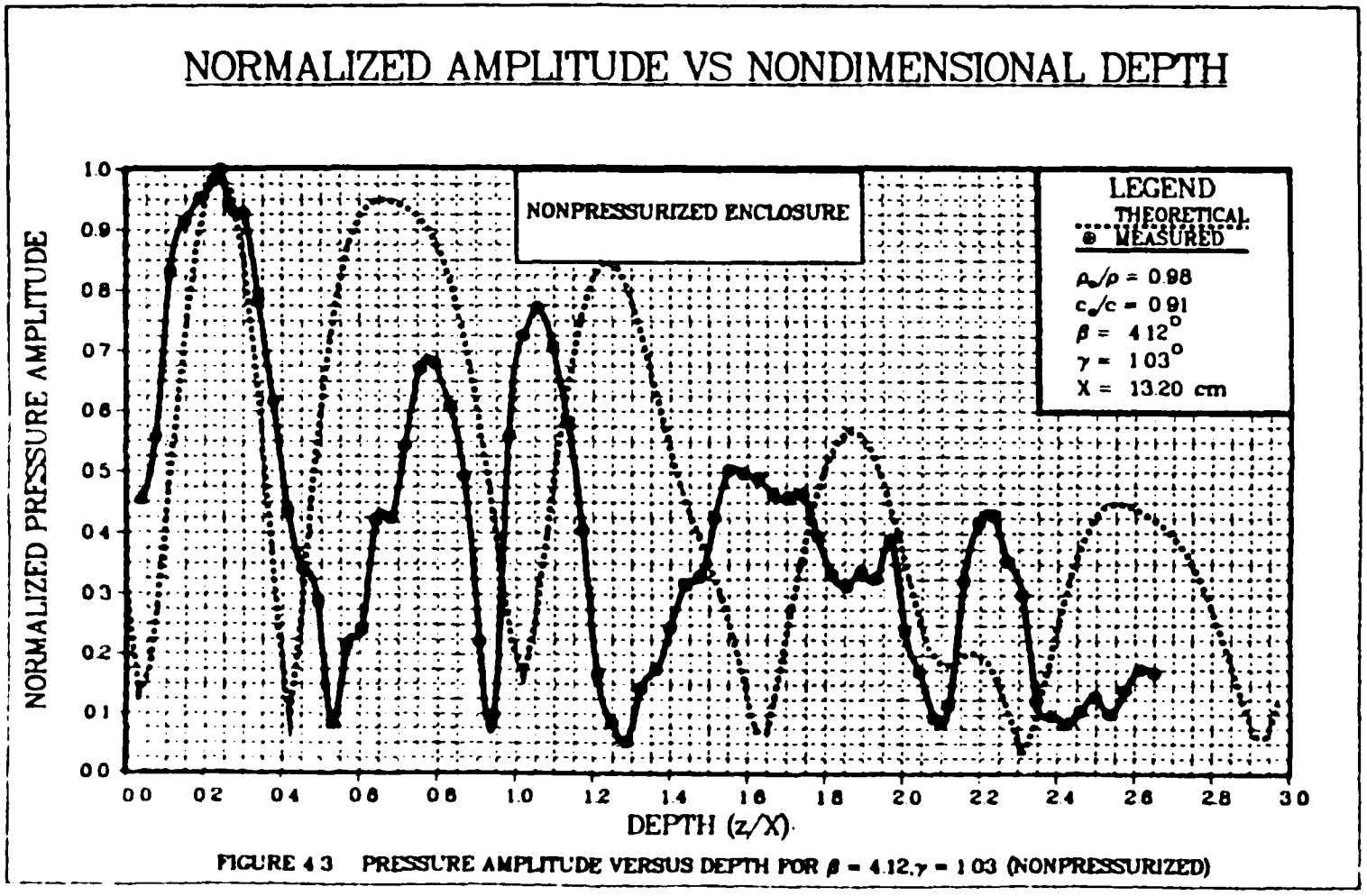

FIGURE 4.3 PRESSURE AMPLITUDE VERSUS DEPTH FOR $\beta = 4.12, \gamma = 1.03$ (NONPRESSURIZED)

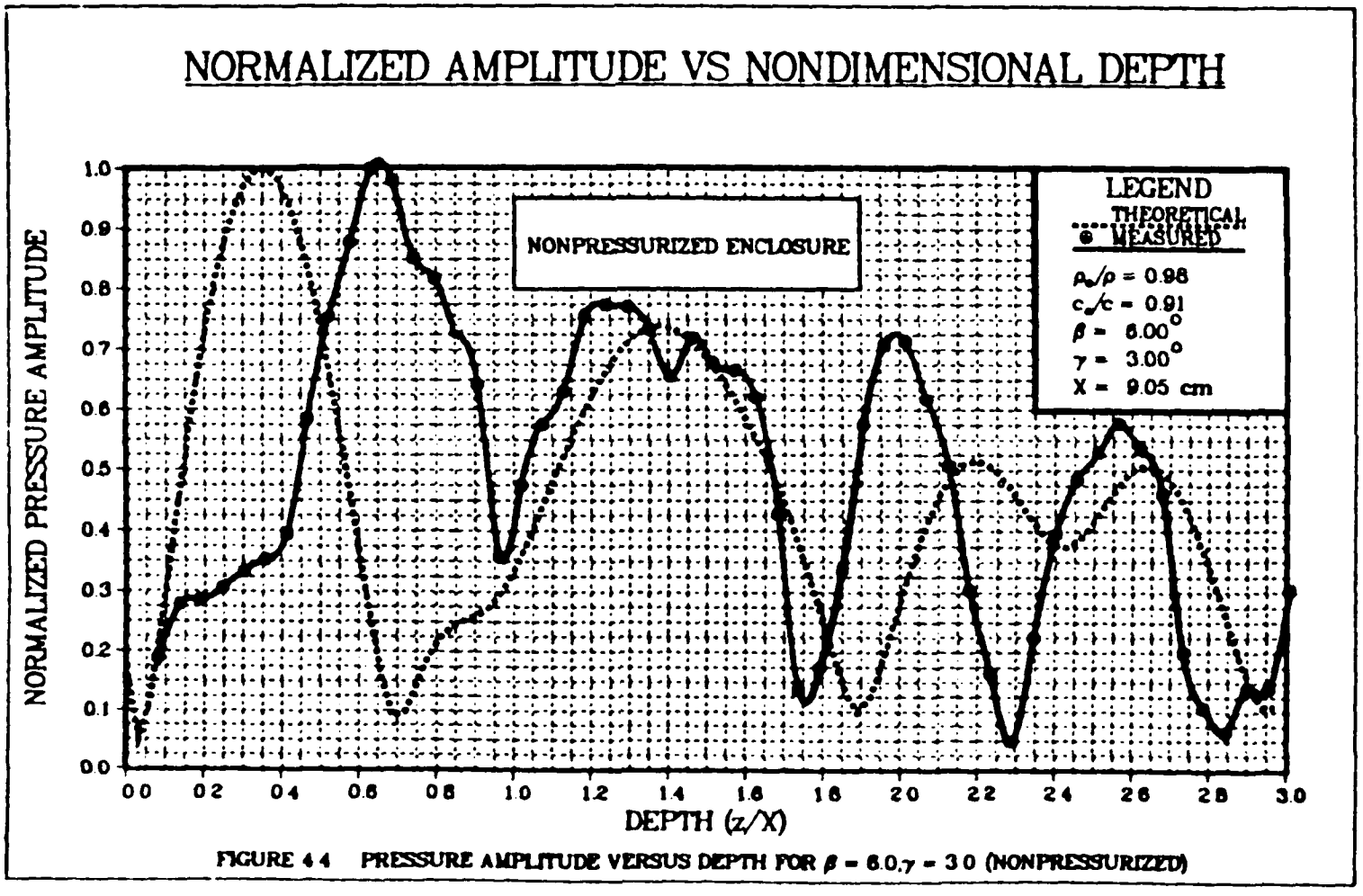

FIGURE 4.4 PRESSURE AMPLITUDE VERSUS DEPTH FOR β = 6.0, γ = 3.0 (NONPRESSURIZED)

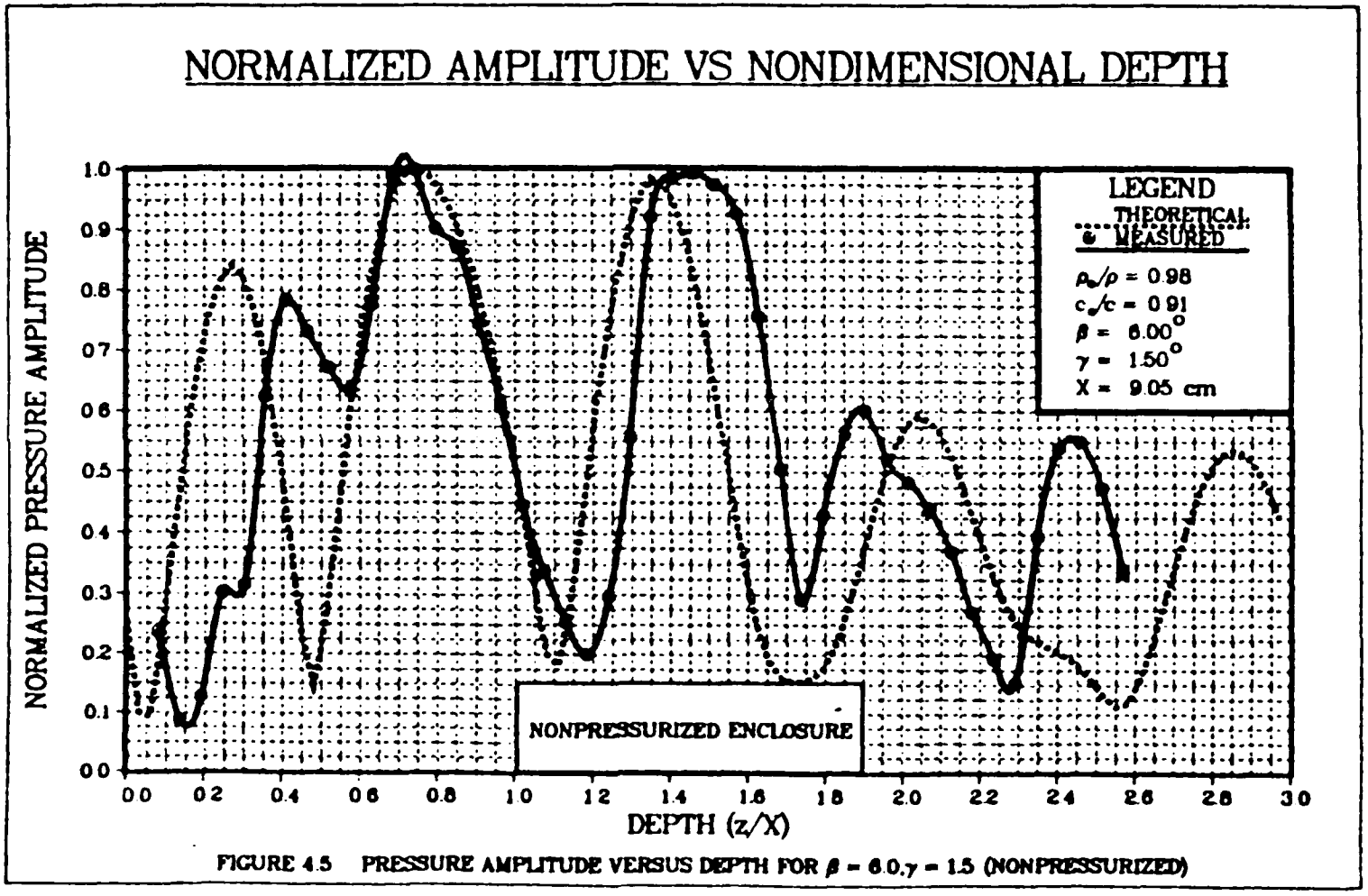

FIGURE 4.5 PRESSURE AMPLITUDE VERSUS DEPTH FOR $\beta = 6.0, \gamma = 1.5$ (NONPRESSURIZED)

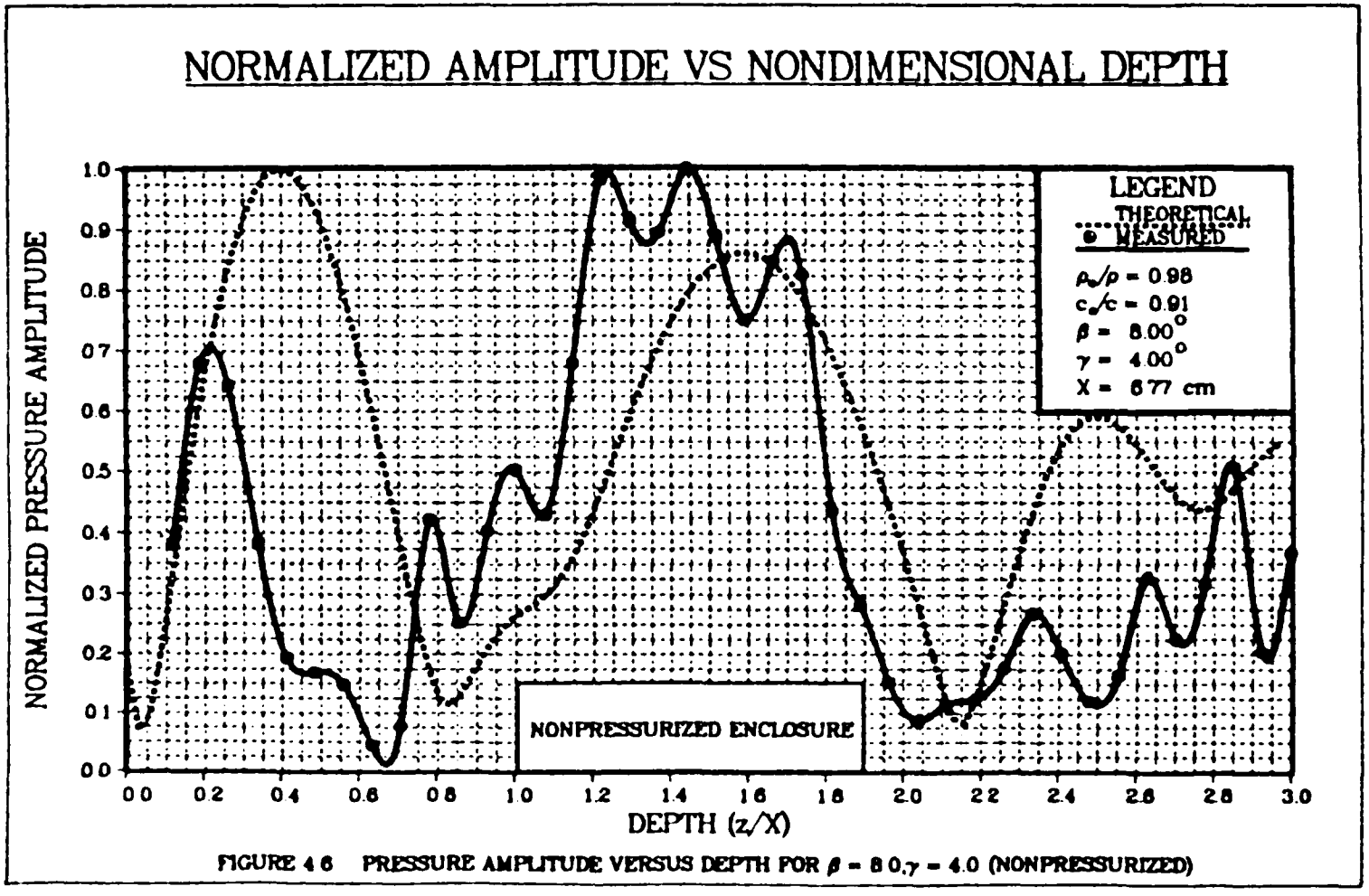

FIGURE 4.6 PRESSURE AMPLITUDE VERSUS DEPTH FOR $\beta = 8.0, \gamma = 4.0$ (NONPRESSURIZED)

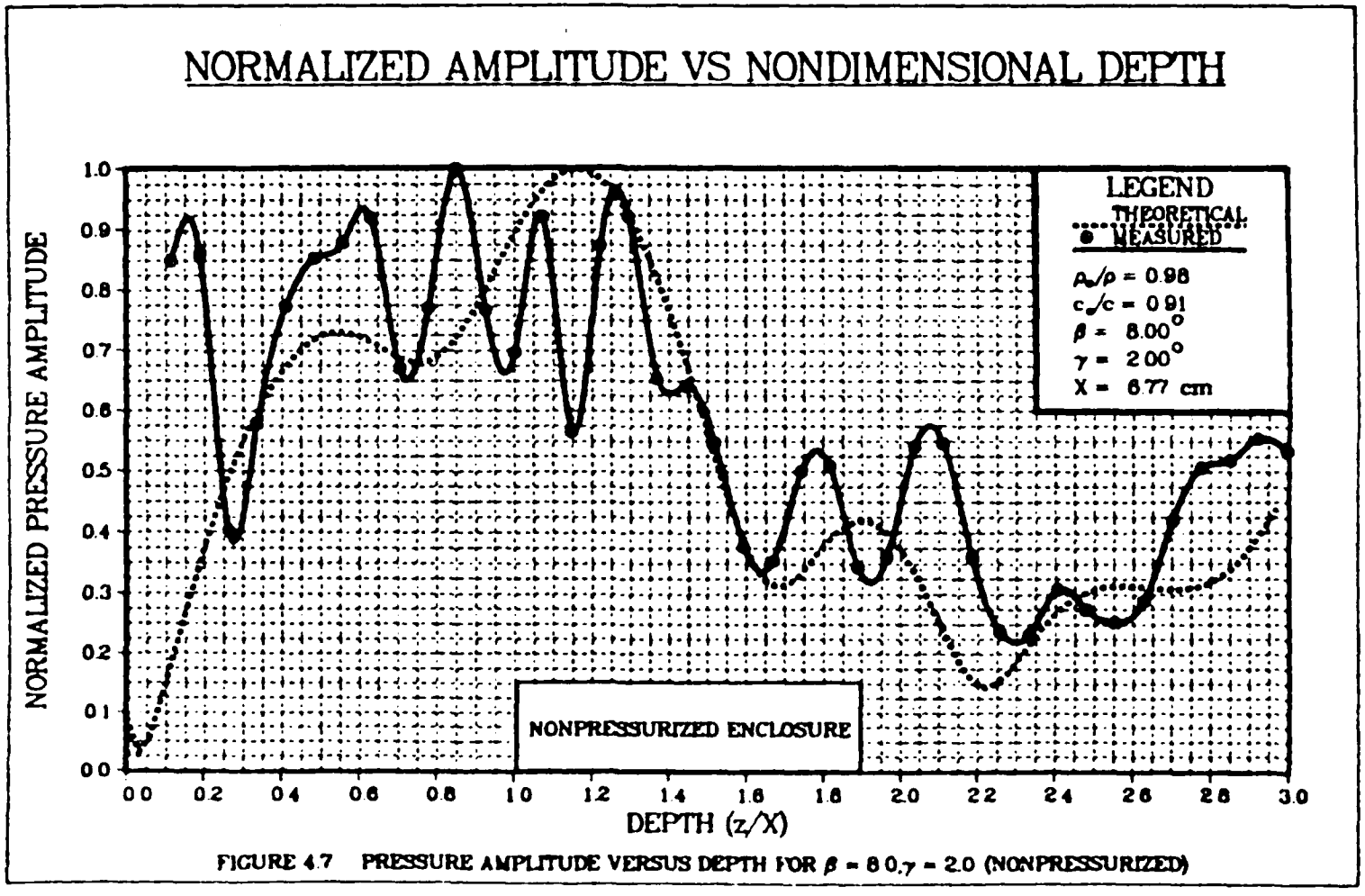

FIGURE 4.7 PRESSURE AMPLITUDE VERSUS DEPTH FOR $\beta = 8.0, \gamma = 2.0$ (NONPRESSURIZED)

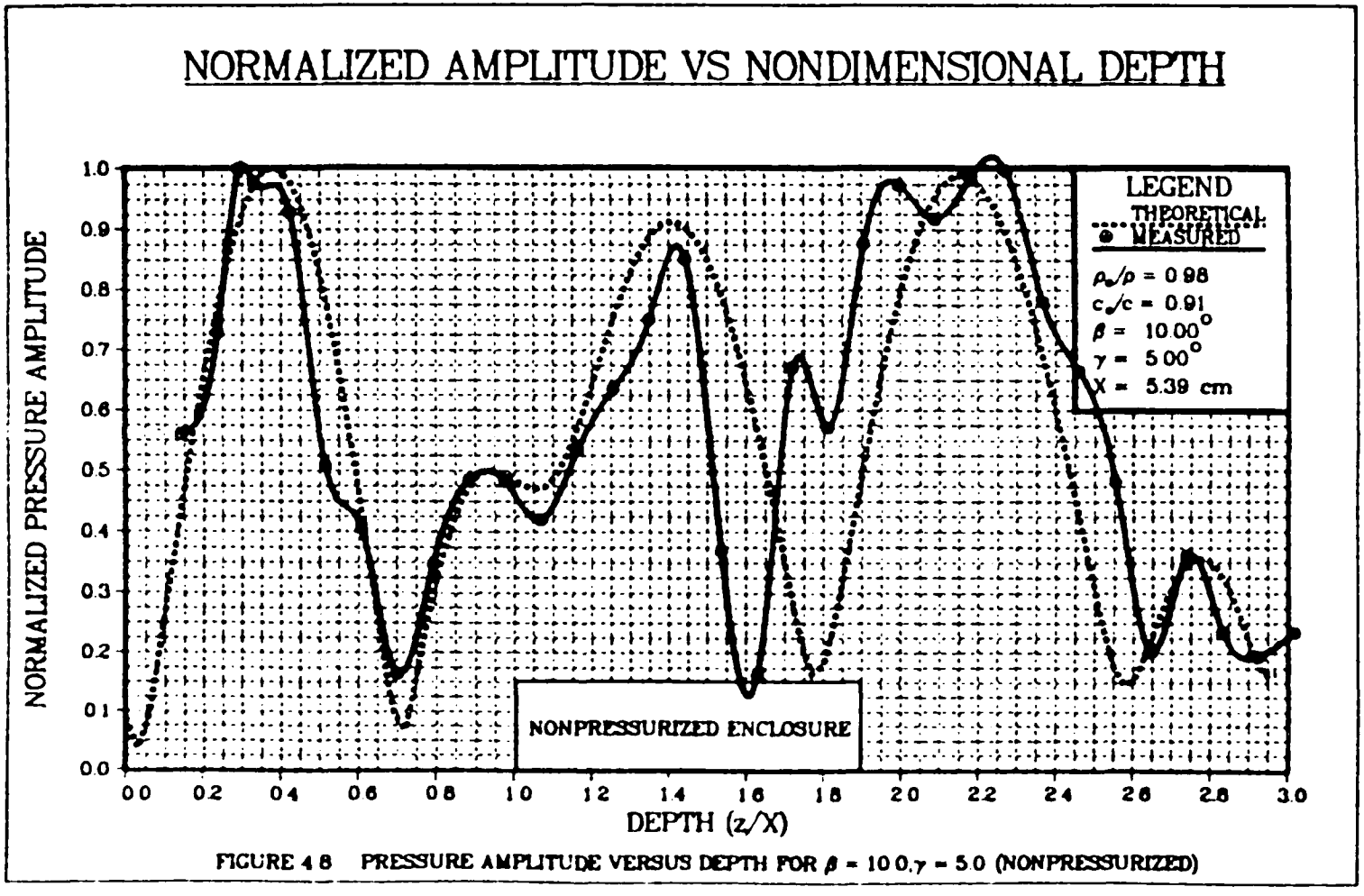

FIGURE 4.8 PRESSURE AMPLITUDE VERSUS DEPTH FOR $\beta = 10.0, \gamma = 5.0$ (NONPRESSURIZED)

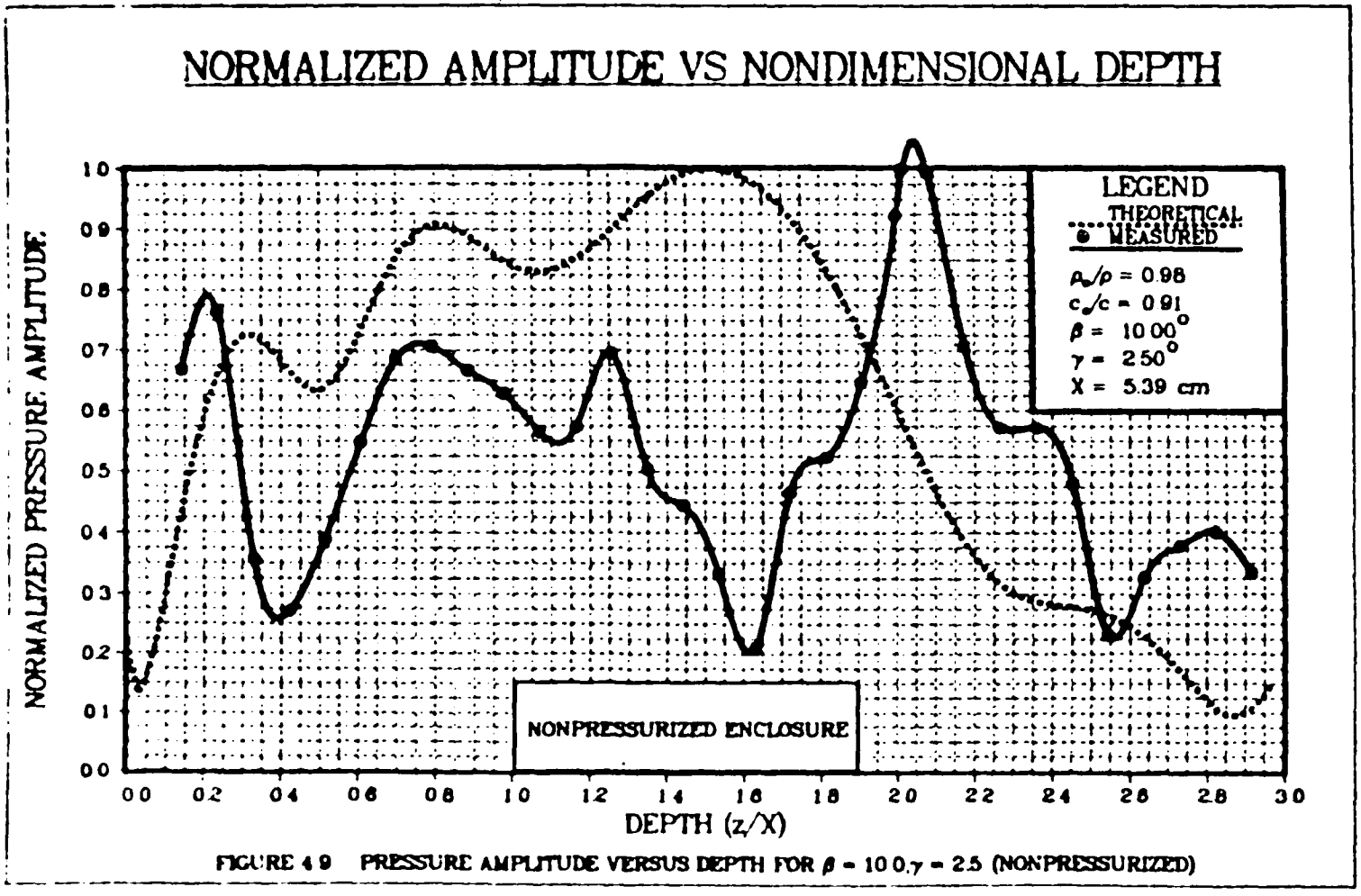

FIGURE 4.9 PRESSURE AMPLITUDE VERSUS DEPTH FOR $\beta = 100, \gamma = 2.5$ (NONPRESSURIZED)

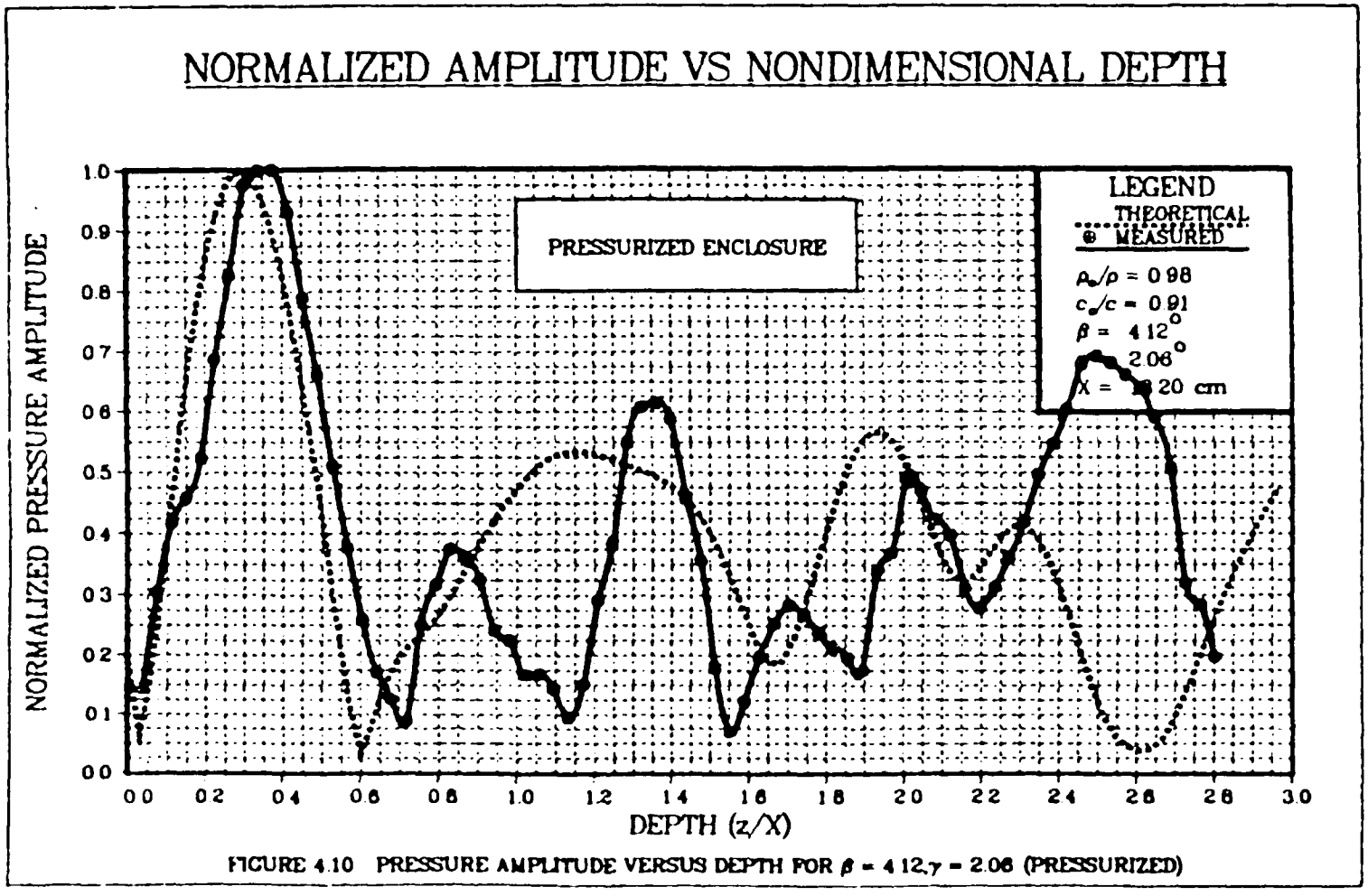

FIGURE 4.10 PRESSURE AMPLITUDE VERSUS DEPTH FOR $\beta = 4.12, \gamma = 2.06$ (PRESSURIZED)

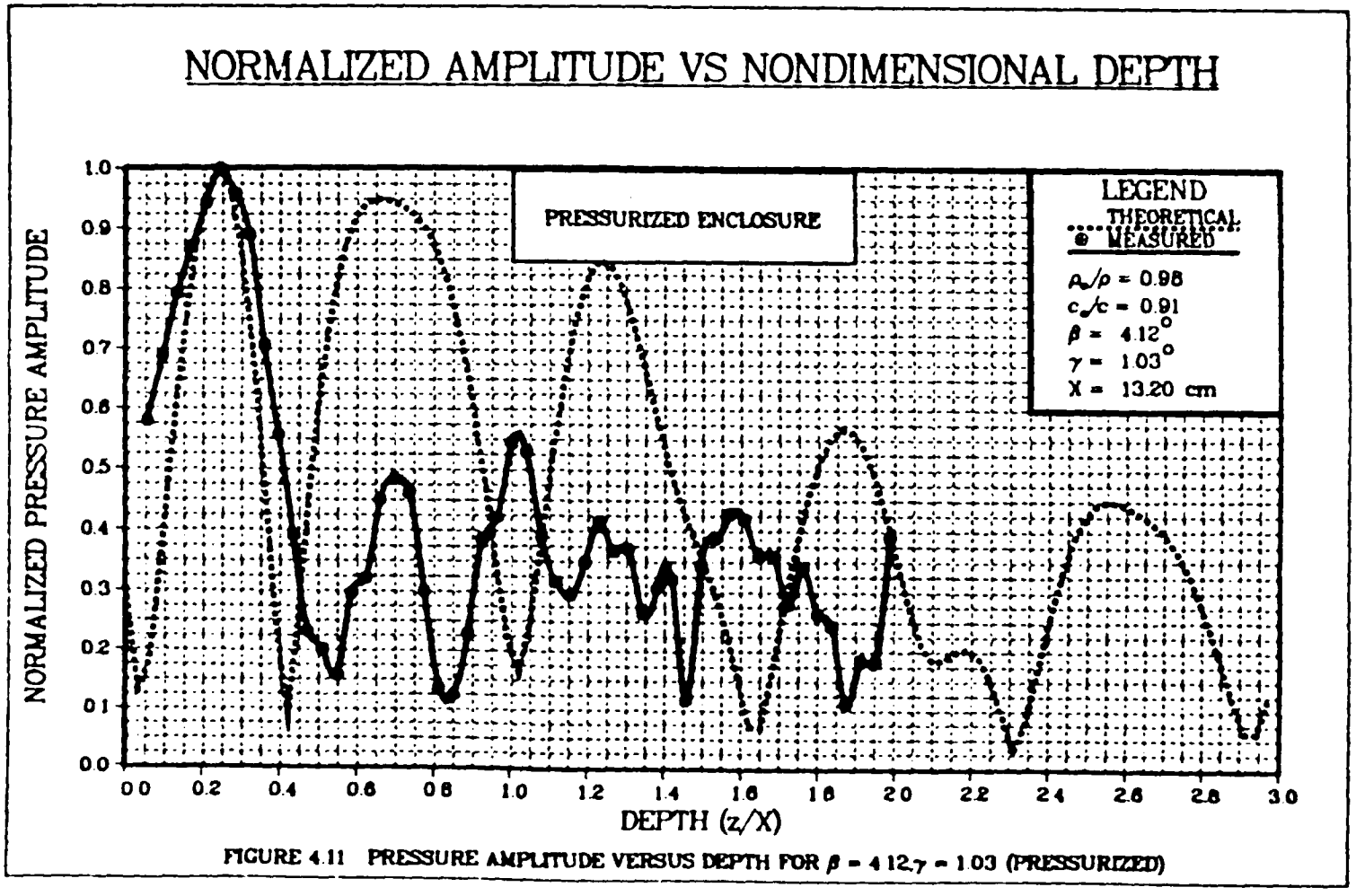

FIGURE 4.11 PRESSURE AMPLITUDE VERSUS DEPTH FOR $\beta = 4.12, \gamma = 1.03$ (PRESSURIZED)

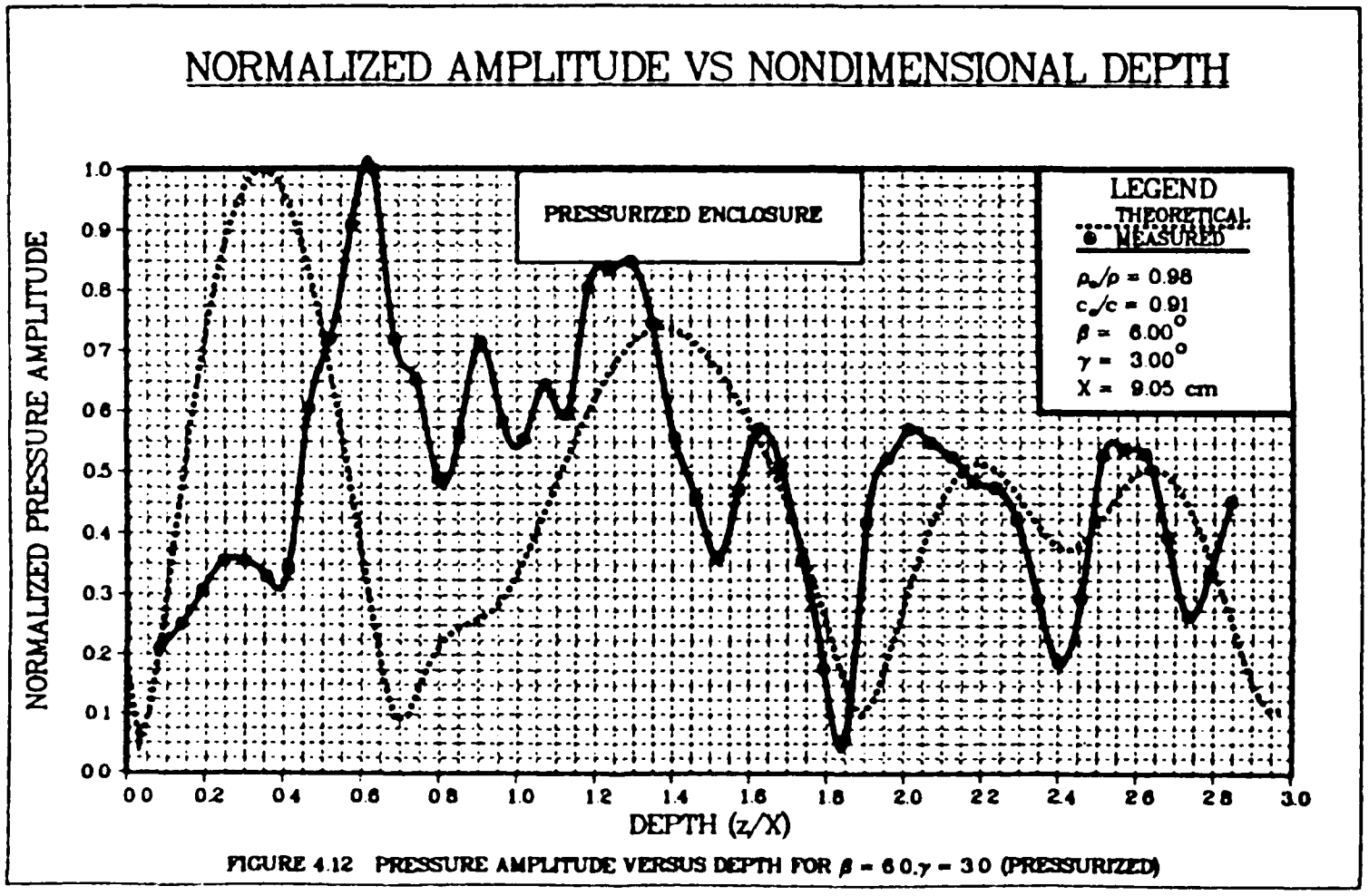

FIGURE 4.12 PRESSURE AMPLITUDE VERSUS DEPTH FOR $\beta = 6.0, \gamma = 3.0$ (PRESSURIZED)

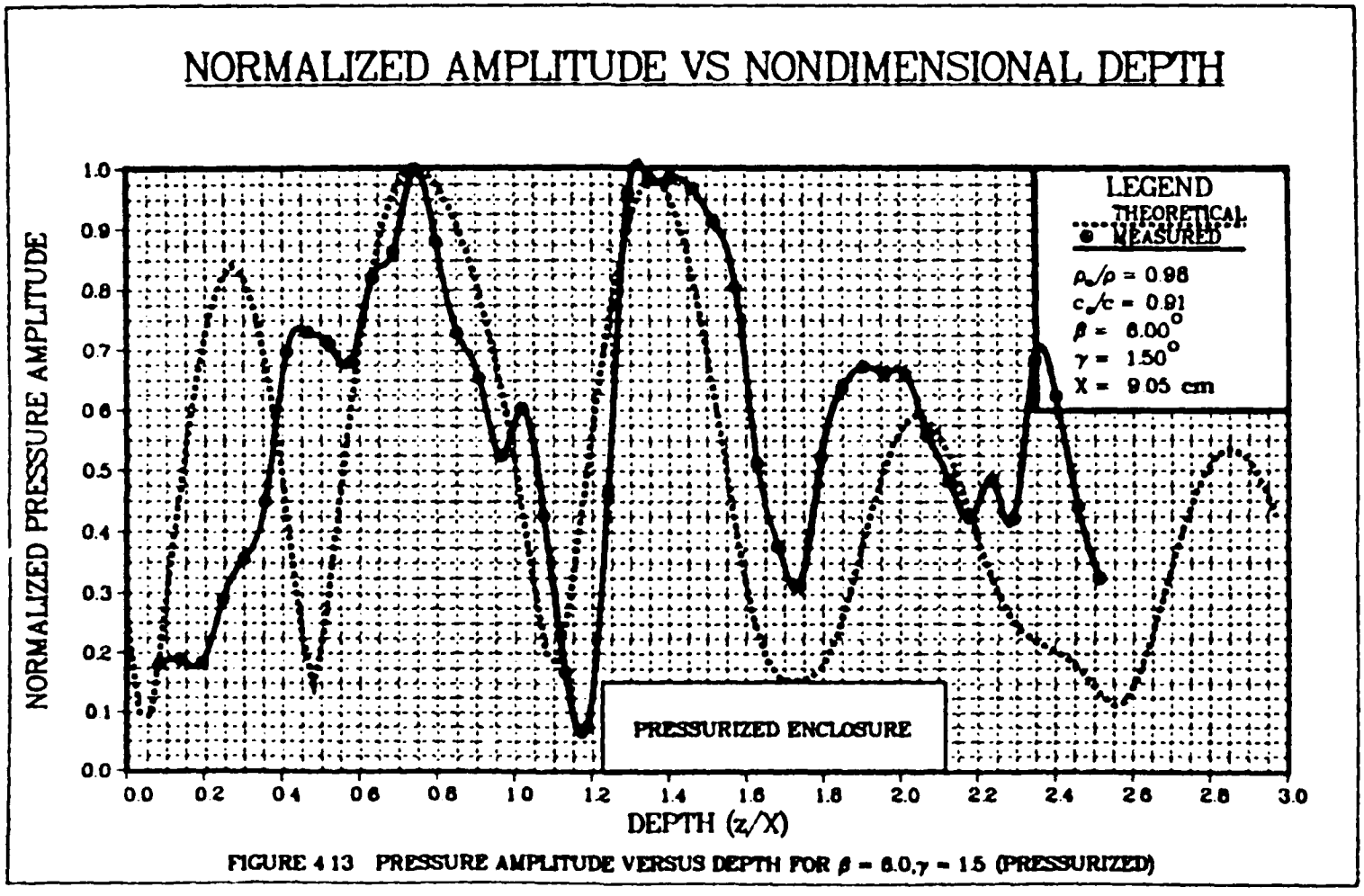

FIGURE 4 13 PRESSURE AMPLITUDE VERSUS DEPTH FOR $\beta = 6.0, \gamma = 1.5$ (PRESSURIZED)

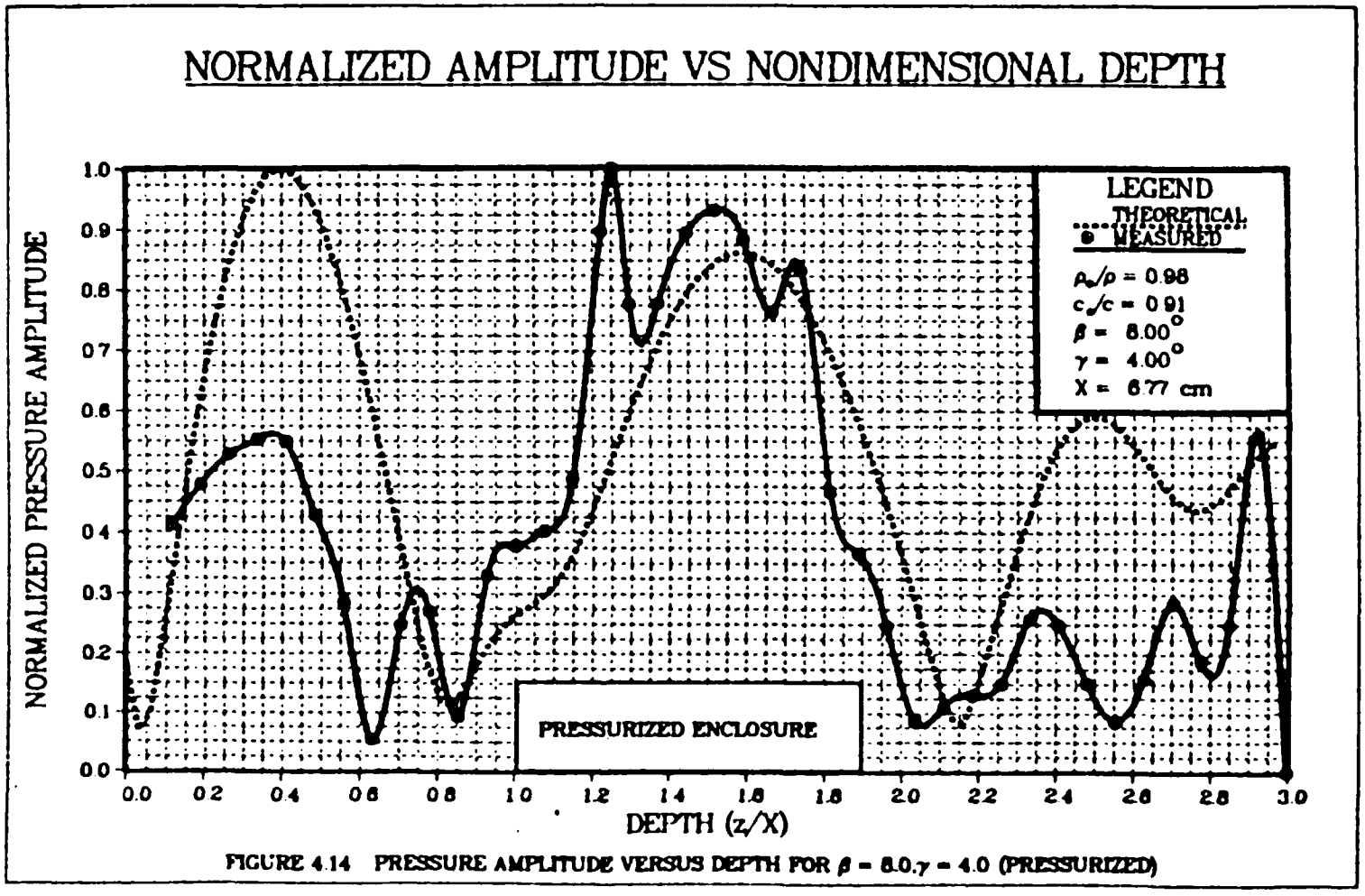

FIGURE 4.14 PRESSURE AMPLITUDE VERSUS DEPTH FOR $\beta = 8.0, \gamma = 4.0$ (PRESSURIZED)

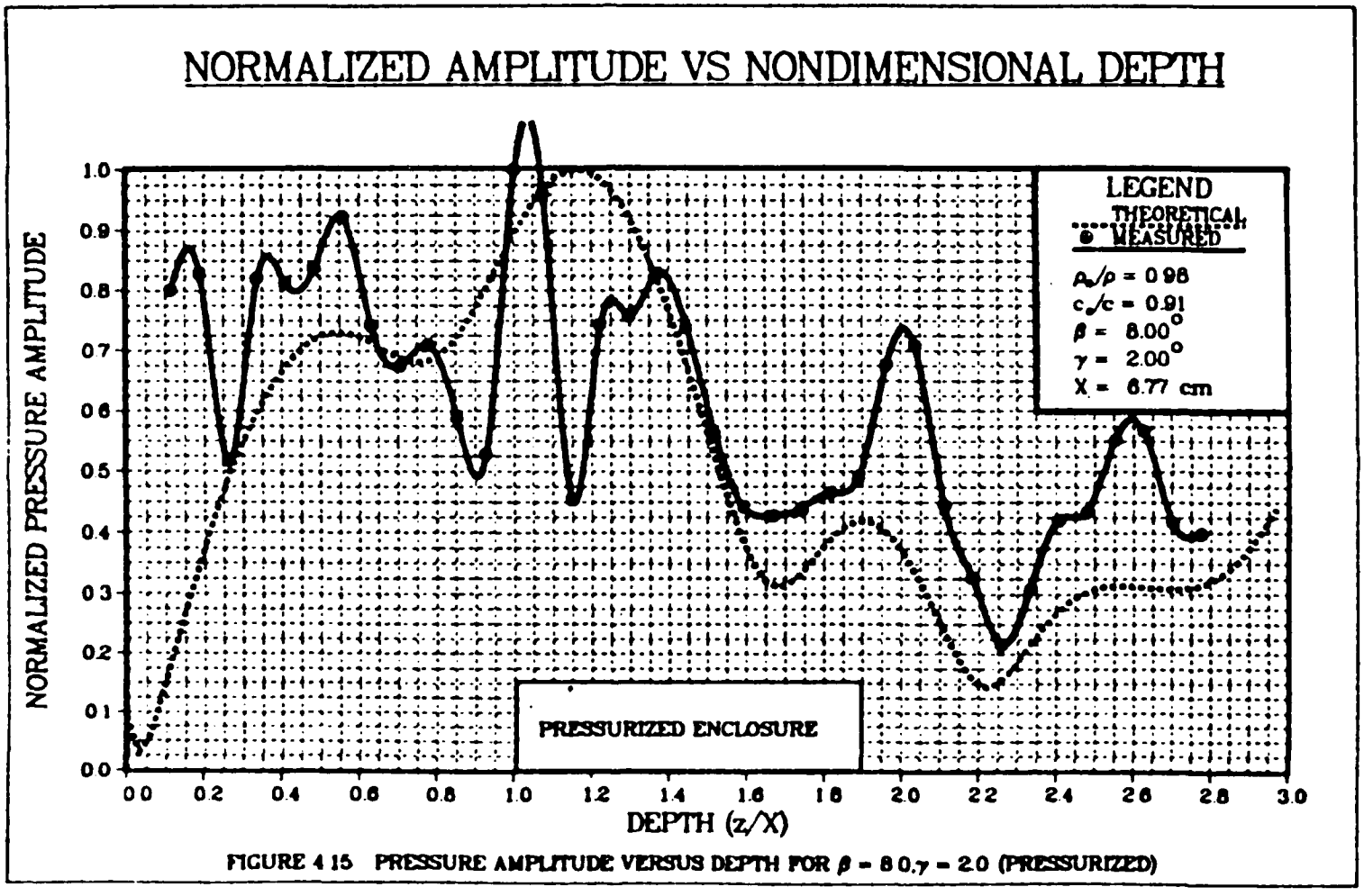

FIGURE 4.15 PRESSURE AMPLITUDE VERSUS DEPTH FOR β = 8.0, γ = 2.0 (PRESSURIZED)

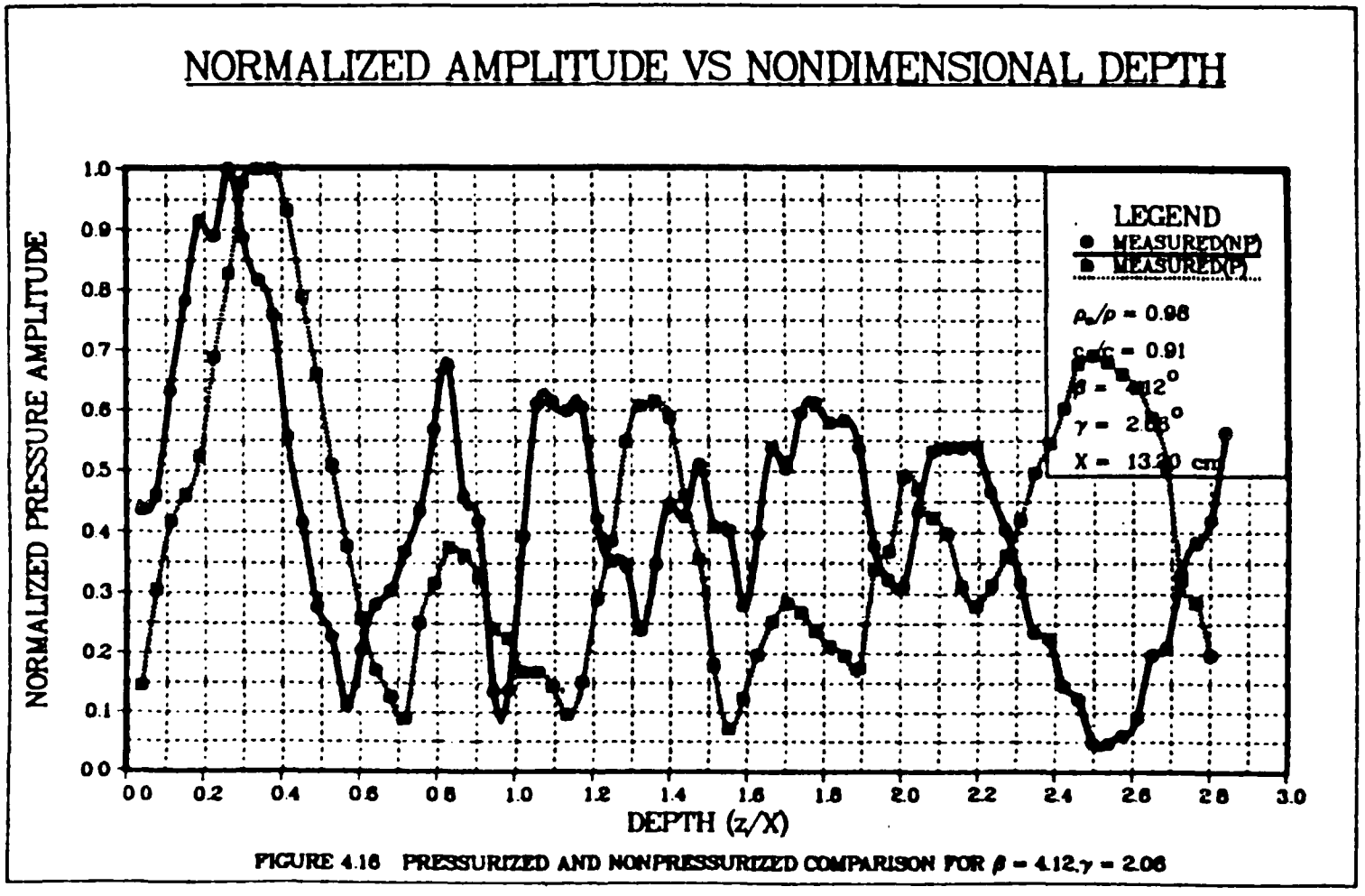

FIGURE 4.16 PRESSURIZED AND NONPRESSURIZED COMPARISON FOR β = 4.12, γ = 2.06

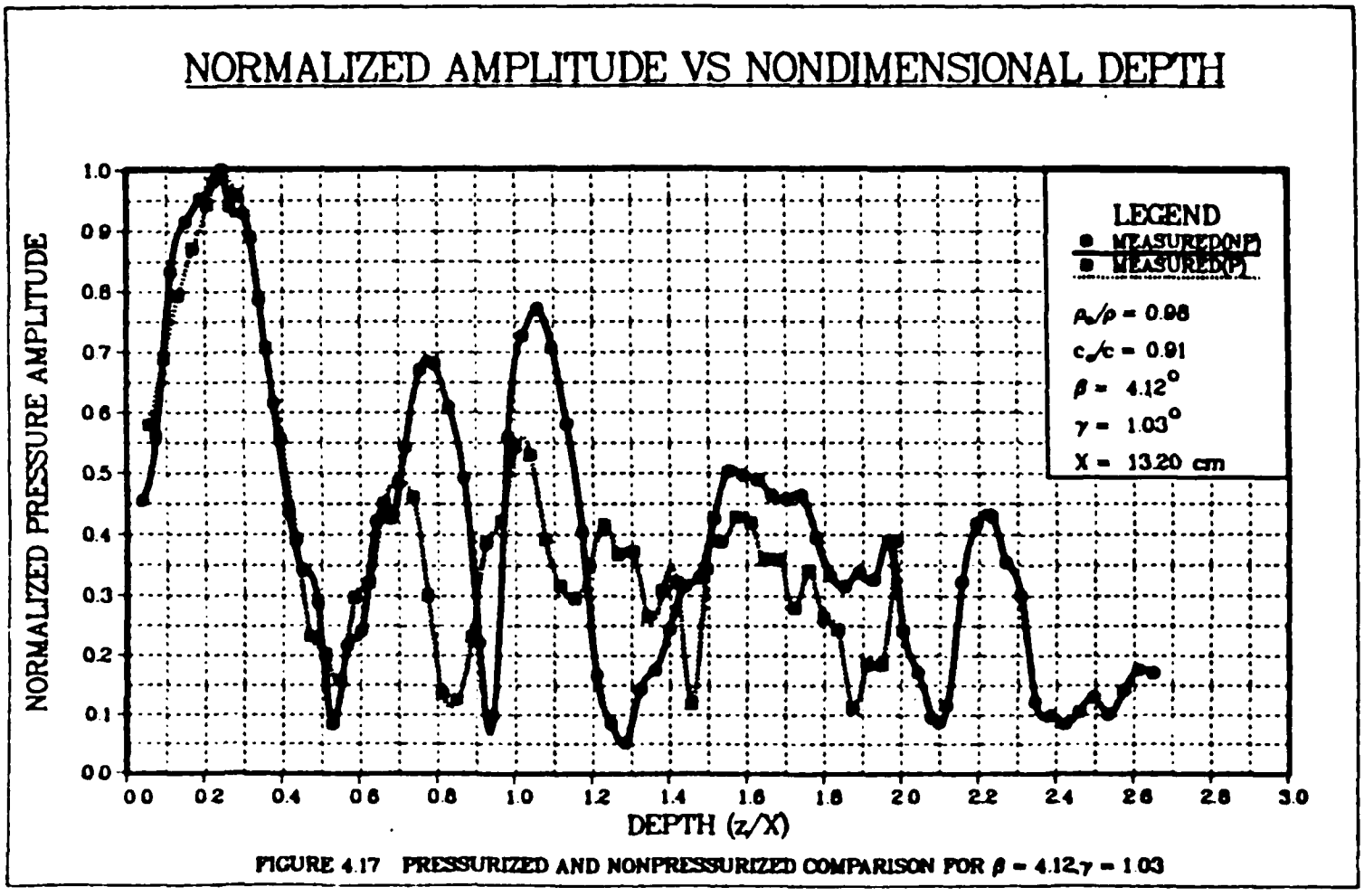

FIGURE 4.17 PRESSURIZED AND NONPRESSURIZED COMPARISON FOR $\beta = 4.12, \gamma = 1.03$

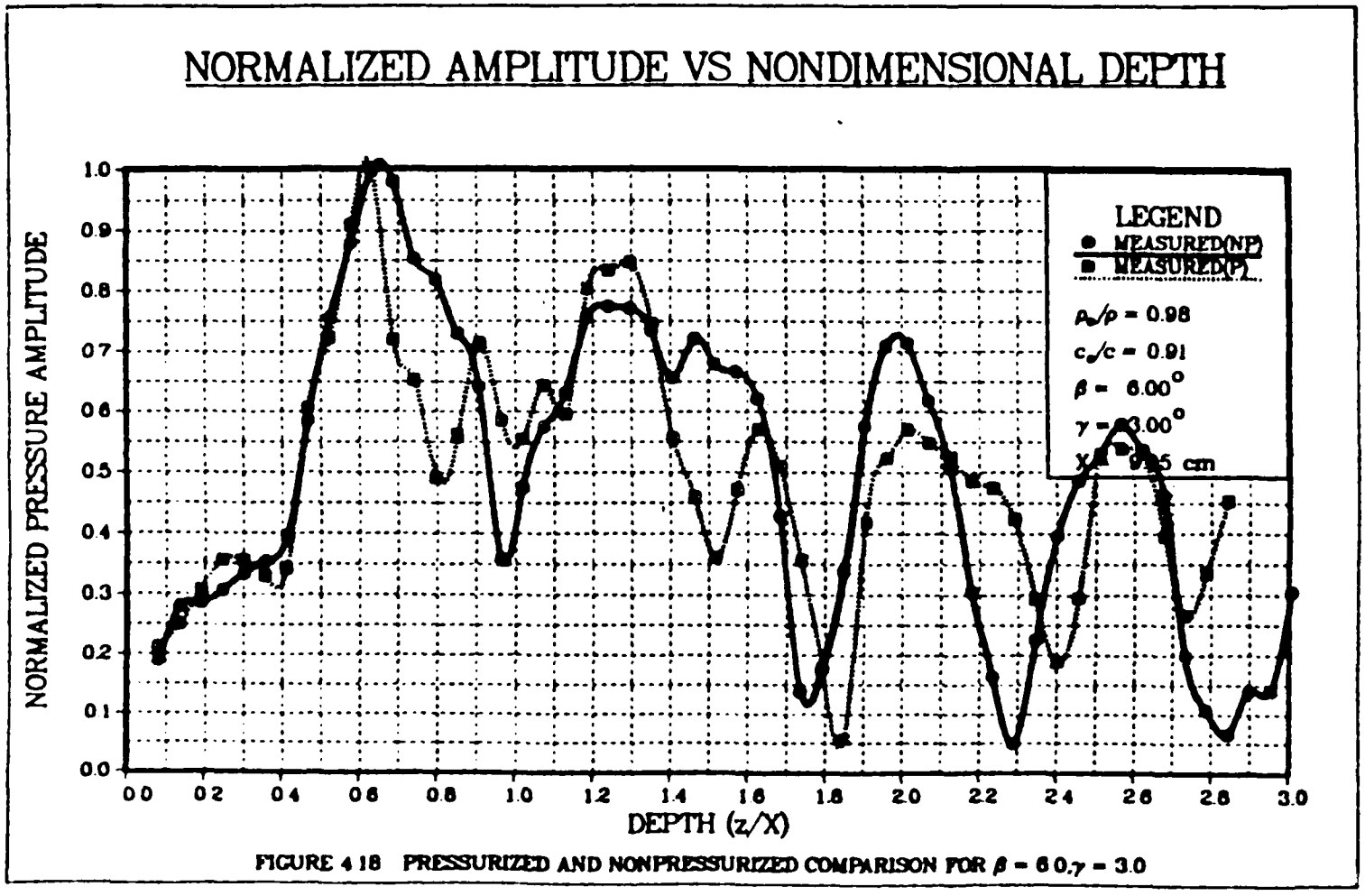

FIGURE 4.18 PRESSURIZED AND NONPRESSURIZED COMPARISON FOR $\beta = 6.0, \gamma = 3.0$

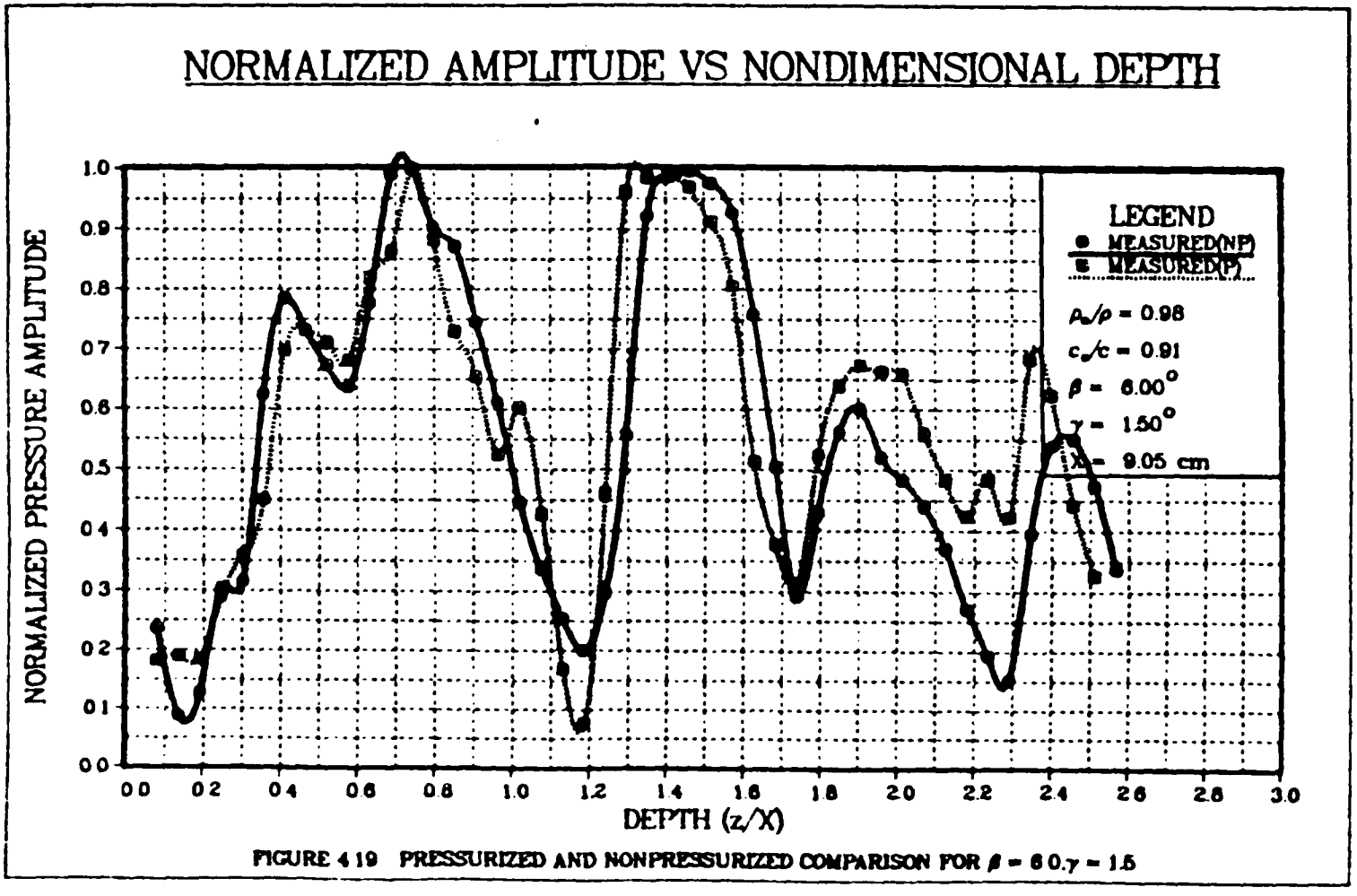

FIGURE 4.19 PRESSURIZED AND NONPRESSURIZED COMPARISON FOR $\beta = 6.0, \gamma = 1.5$

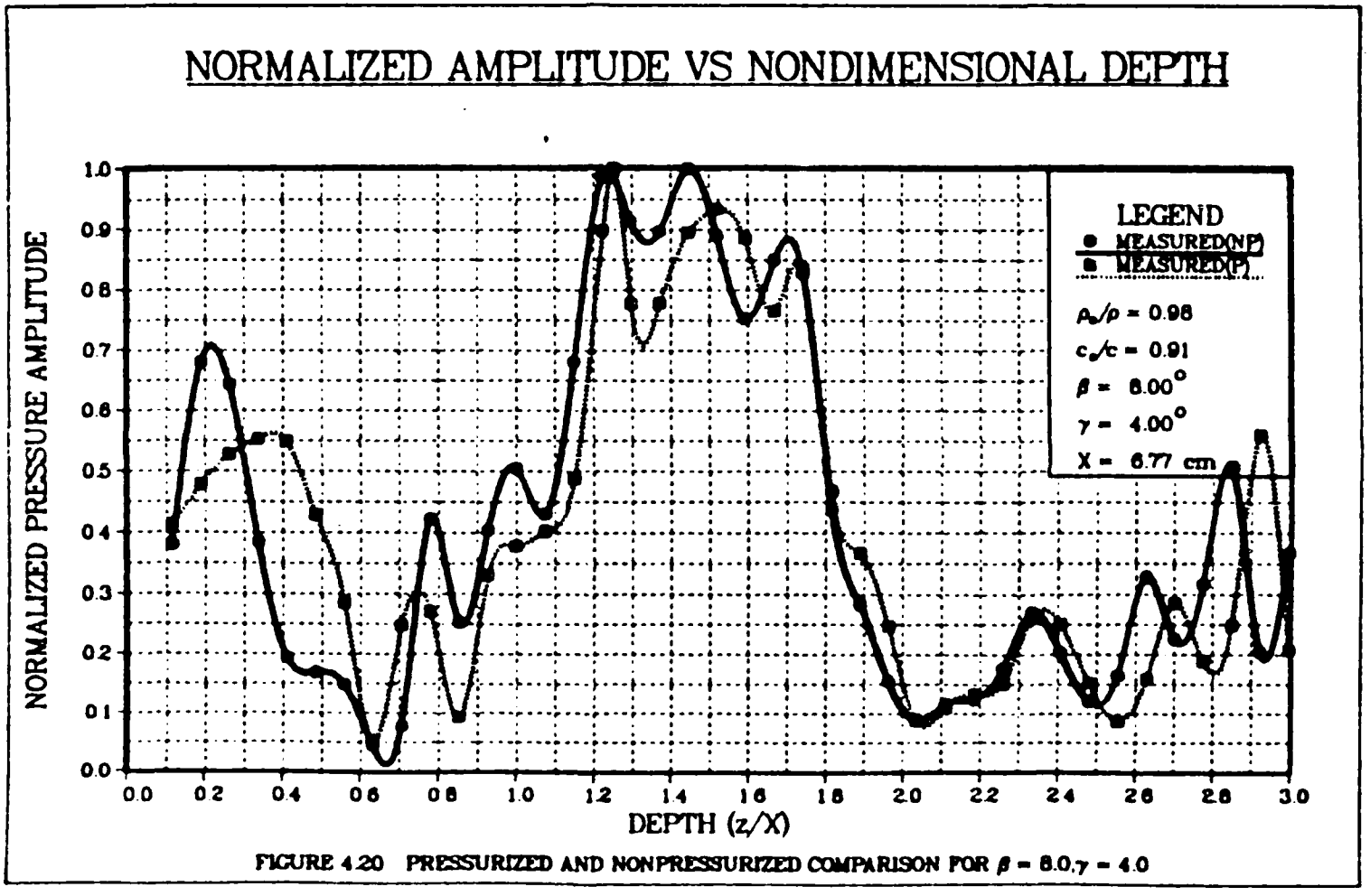

FIGURE 4.20 PRESSURIZED AND NONPRESSURIZED COMPARISON FOR $\beta = 8.0, \gamma = 4.0$

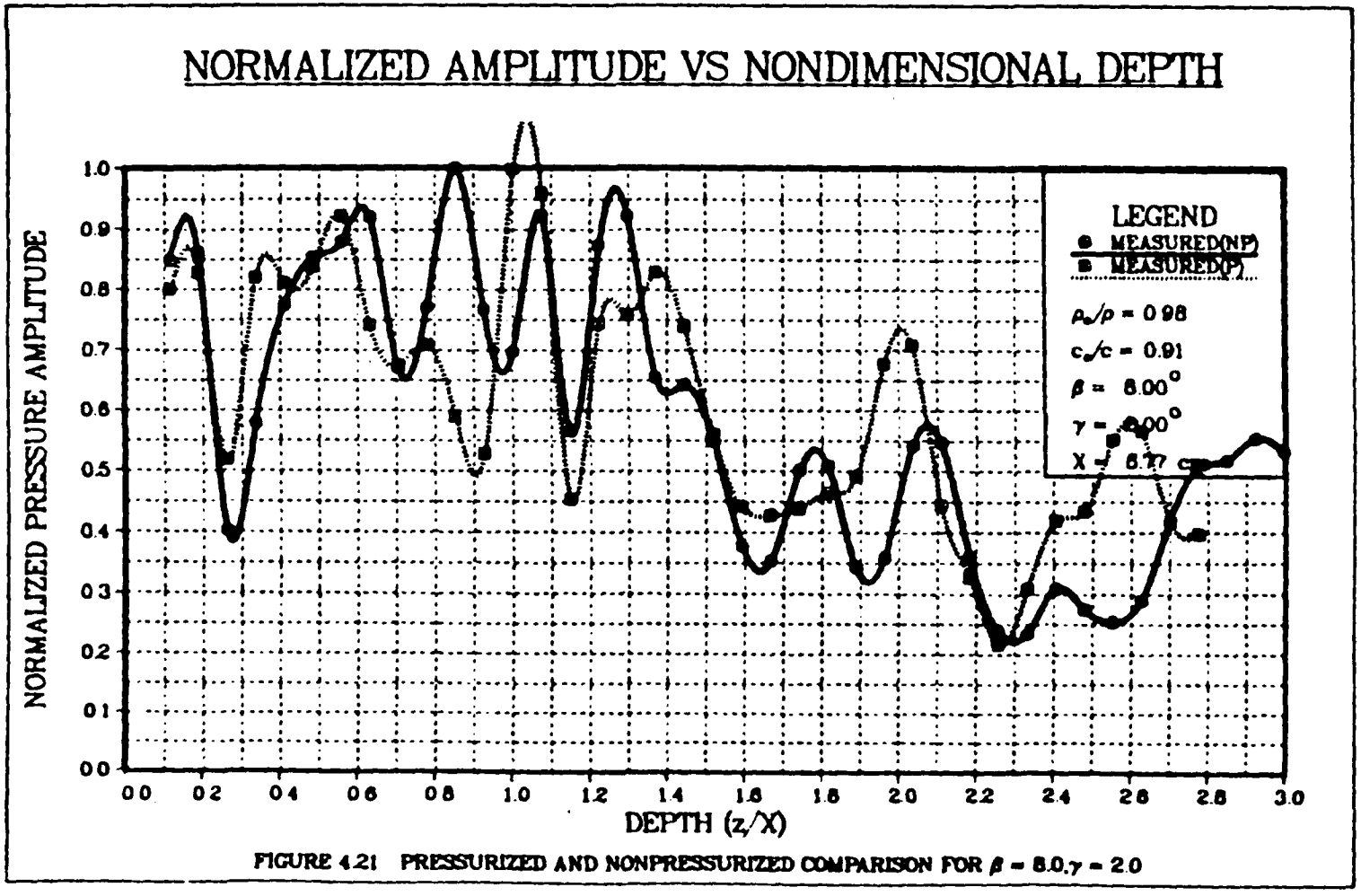

FIGURE 4.21 PRESSURIZED AND NONPRESSURIZED COMPARISON FOR $\beta = 8.0, \gamma = 2.0$

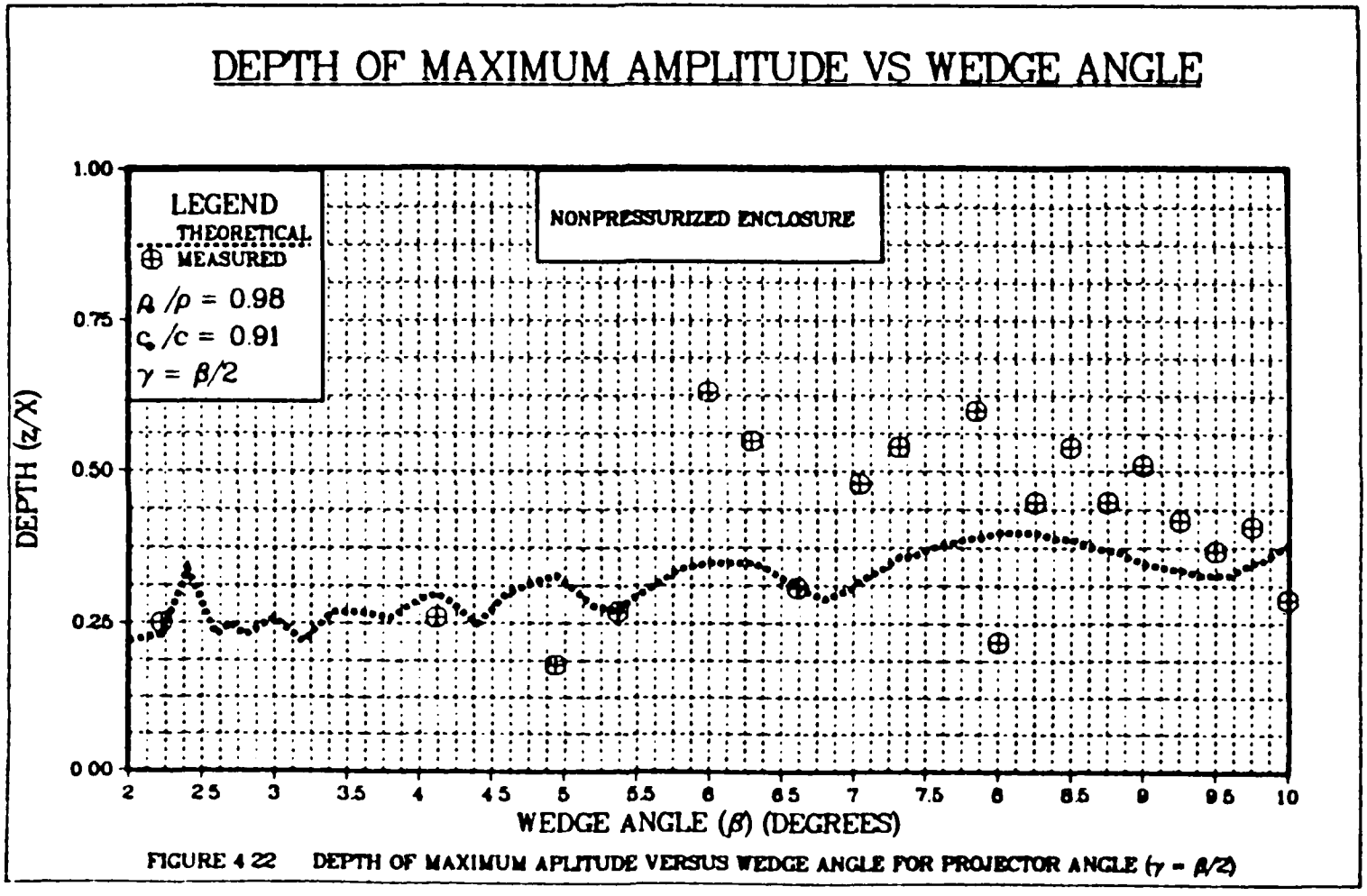

FIGURE 4.22 DEPTH OF MAXIMUM APLITUDE VERSUS WEDGE ANGLE FOR PROJECTOR ANGLE ($\gamma = \beta/2$)

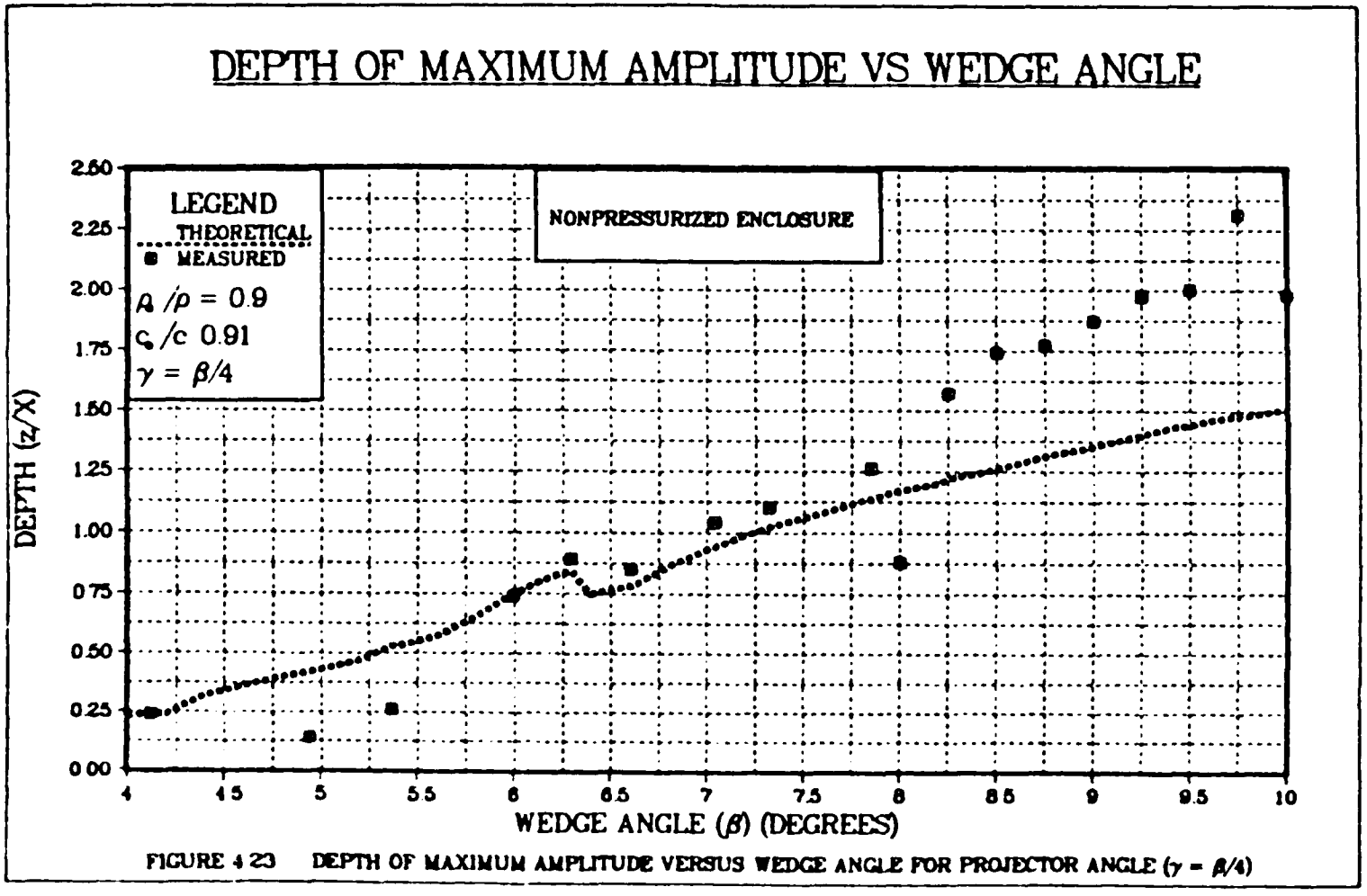

FIGURE 4.23 DEPTH OF MAXIMUM AMPLITUDE VERSUS WEDGE ANGLE FOR PROJECTOR ANGLE ($\gamma = \beta/4$)

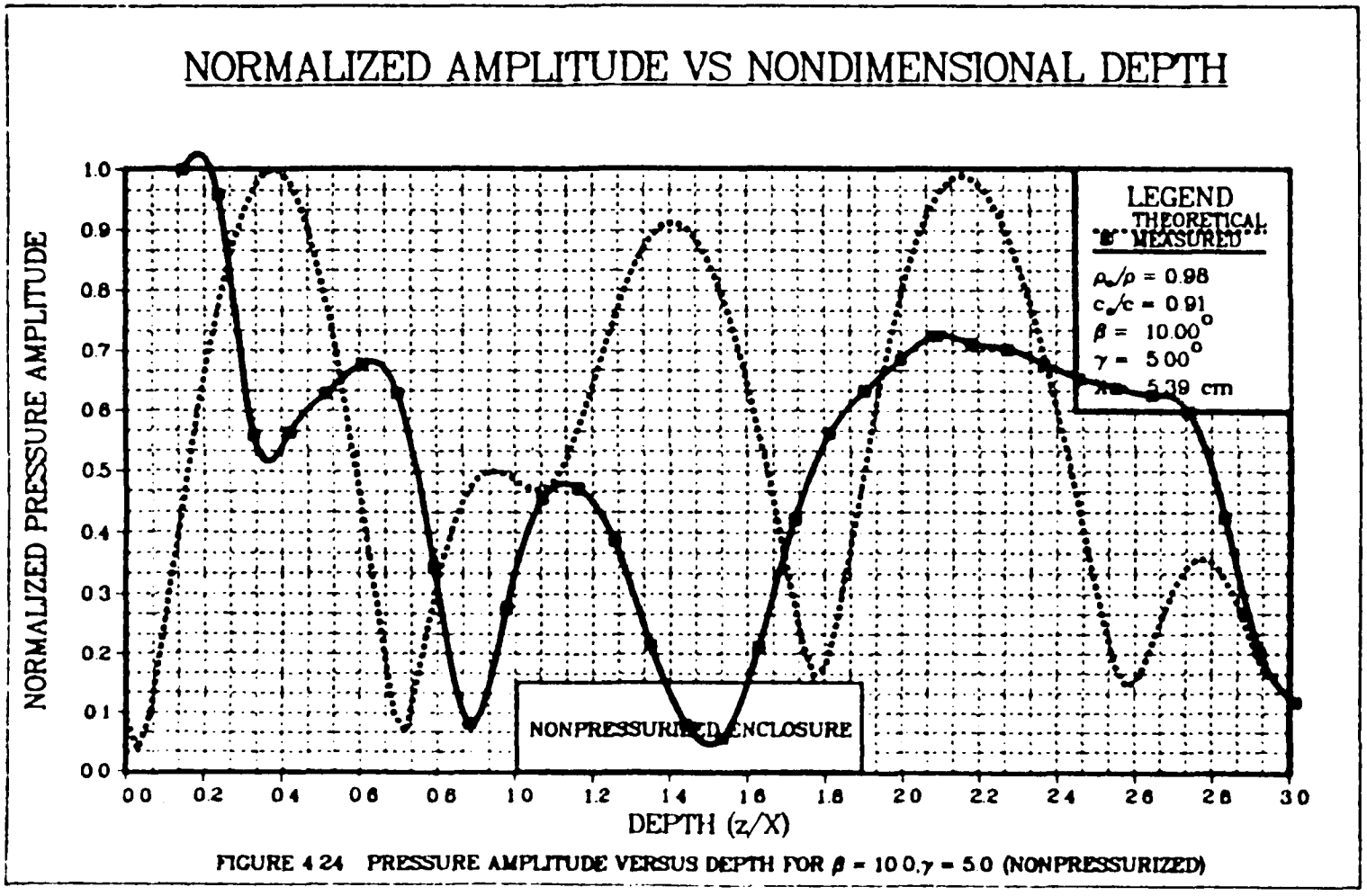

FIGURE 4.24 PRESSURE AMPLITUDE VERSUS DEPTH FOR $\beta = 10.0, \gamma = 5.0$ (NONPRESSURIZED)

V. CONCLUSIONS

The experimental data confirms that the pressure profile beneath the apex of a fluid wedge overlying a fast bottom is a highly structured sound field. In general, the profile presents a first maximum (usually the maxium pressure amplitude) at a relatively shallow depth and then experiences a succession of minima and maxima. In a significant number of instances the depth at which the maximum pressure occurred matched the predicted depth. The remainder of the profile was usually displaced toward deeper depths with their maxima rarely achieving the pressure amplitudes predicted. On the other hand, the minima occurred consistently at the same depth and amplitude as predicted. Although wedge angles of 4.12 and 8.0 degrees exhibited several erratic phase interference patterns in the region of the second maximum, the overall similarities between the experimental and predicted curves is unmistakable.

The depth at which the maximum pressure occurred remained relatively constant throughout the wedge angles from two to ten degrees when the projector elevation angle was set at one-half the wedge angle. When the projector was repositioned to an elevation angle of one-quarter the wedge angle, the data demonstrated that the depth of maximum pressure increased steadily as the wedge angle increased. Thus, for both projector elevation positions experimental and theoretical predictions were in agreement.

Analysis of the results between the pressurized and nonpressurized conditions reveals that the data is in agreement with each other but, that the data obtained during nonpressurized conditions were the preferred data when

compared against theory. This conclusion was not anticipated. The difference in the densities of the fluids demanded that a downward force was required to counteract the superior hydrostatic force acting upward on the Mylar membrane. The only plausible explanation is that the enclosure must have been overpressurized, thus altering the geometrical parameters, wedge angle and projector elevation angle. The data shows an improvement between the curves of the two conditions as wedge angle increased. This improvement is attributed to the proficiency in techniques required to set the proper gecmetric parameters, rather than indicating that agreement was obtained at a particular angle or to the overall increasing of the wedge angle.

Particularly interesting are the results obtained in the eight degree angle. Both pressurized and nonpressurized conditions are in agreement. Yet, they demonstrate several distinct differences with the predicted profile. First, at the predicted depth of the pressure maximum, experimental data indicates that a maximum exists, but the pressure amplitude is 30 to 45 percent below the prediction. Secondly, the data indicates that the depth of maximum pressure occurs at the depth of the second largest maximum. The maximum pressure is 15 percent greater than predicted at that depth location. Clearly, experimental error could be the culprit, however, four accepted data events and several additional measurements were conducted and all confirmed the measured results. This implies that additional interference mechanisms are at work at this wedge angle. Although profiles for the angles between 8.0 and 10.0 degrees were not investigated thoroughly, indications suggest that similar problems exist.

The relocation of the projector to a position closer to the apex affected the pressure profile. The measured data does not resemble the predicted curve except that the depths

of maximum pressure do occur near one another in the shallow depth region. This is not surprising in that less energy is allowed to transfer to the substrate, thus reducing the potential interference caused by the individual beams of sound.

A final note regarding the pressure field beneath the apex is required. As Receiver B was lowered in the water, its acoustic center would occasionally swing off the vertical plane of the projector's acoustic axis. It was observed that at depths of pressure maxima the pressure observed on either side of the vertical plane was less than, but near the value of the maximum. However, at depths were a minimum was observed the surrounding region indicated very much higher amplitudes. Rarely did a minimum occur on the entire horizontal plane, while on several occasions it did not matter if the receiver was perfectly aligned on the vertical plan of the acoustical axis because the entire horizontal plane was at the same maximum amplitude.

VI. RECOMMENDATIONS

The following recommendations are provided to improve the equipment facility and thus, improving upon the precision and accuracy of the experiment:

A. A mechanical device is needed which would lower the receiver in the water while maintaining its alignment in the vertical plane of the projector's acoustic axis. The number of data points required to complete a data event was a function of wedge angle and ranged from 74 to 32 points. The time to make those measurements was from 4 to 7 hours, but more importantly it required continuous blocks of time when the parameters and electronic equipment were stable. Manually lowering the receiver creates depth and alignment errors while reducing valuable time which should be reserved for follow-up readings to verify the data.

B. Although visual integration was a viable way to measure the data, an HP 85 computer with the interface to tap into the Nicolet oscilloscope would provide rapid data collection and assessment while making significant gains in accuracy. The addition of computerized data taking should be made in conjunction with the mechanical device recommended above.

C. The Mylar membrane has proven on a number occasions that it possesses the tensile strength to separate the liquids and not rupture. In order to reduce bottom reflections the enclosure should be suspended over a large anechoic water tank instead of the wooden tank.

D. Pressurizing the enclosure is still believed to be the most viable method of ensuring that the forces acting on the membrane are equalized. Therefore, a manometer should be installed to accurately control the pressure within the enclosure.

E. The computer model should be revised to account for a source at a finite distance and to accept the correct absorption input. A value of 0.001 was used for the predicted data, however the correct value was 0.0000005. Additionally, it would be most convenient if the program allowed an entire range of variables to be accepted at one time. Presently only one set of parameters are accepted, thus requiring excessive amounts of time to retrieve predicted results for an entire range of wedge angles, one angle at a time.

LIST OF REFERENCES

1. Coppens, A. B., Humphries, M., and Sanders J. V., "Propagation of Sound out of a Fluid Wedge into an Underlying Fluid Substrate of Greater Sound Speed," The Journal of the Acoustical Society of America, v. 76, pp. 1456-1465, November 1984.

2. Edwards, J. N., Jr., A Preliminary Investigation of Acoustic Energy Transmission From a Tapered Fluid Layer Into a Fast Bottom, M.S. Thesis, Naval Postgraduate School, Monterey, California, 1976.

3. Netzorg, G. B., Sound Transmission from a Tapered Fluid Layer into a Fast Bottom, M.S. Thesis, Naval Postgraduate School, Monterey, California, 1977.

4. Kawamura, M. and Ioannou, I., Pressure on the Interface Between a Converging Fluid Wedge and a Fast Fluid Bottom, M.S. Thesis, Naval Postgraduate School, Monterey, California, 1978.

5. Naval Postgraduate School 61-79-002, Two Computer Programs for the Evaluation of the Acoustic Pressure Amplitude and Phase at the Bottom of a Wedge-Shaped, Fluid Layer Overlying a Fast Fluid Half Space, by A. B. Coppens and others, December 1978.

6. Kinsler, L. E., Frey, A. R., Coppens A. B., and Sanders J. V., Fundamentals in Acoustics, Wiley, 1982.

7. Macpherson, J. D, and Daintith, M. J., "Practical Model of the Shallow-Water Acoustic Propagation," The Journal of the Acoustical Society of America, v. 41, pp. 850-854, 1966.

8. Baek, C. K., The Acoustic Pressure in a Wedge-Shaped Water Layer Overlying a Fast Fluid Bottom, M.S. Thesis, Naval Postgraduate School, Monterey, California, 1984.

9. Ziomek,L., Lecture nctes from Sonar Systems Engineering course, Naval Postgraduate School, Monterey, 1984

BIBLIOGRAPHY

Coppens, A. B., Notes from Underwater Acoustics class, Naval Postgraduate School, Monterey, 1984.

INITIAL DISTRIBUTION LIST

No.		Copies
1.	Defense Technical Information Center Cameron Station Alexandria, Virginia 22314	2
2.	Library, Code 0142 Naval Postgraduate School Monterey, California 93943	2
3.	Superintendent ATTN: Dr. A. B. Coppens, Code 61Cz Naval Postgraduate School Monterey, California 93943	2
4.	Superintendent ATTN: Dr. J. V. Sanders, Code 61Sd Naval Postgraduate School Monterey, California 93943	5
5.	Chief of Naval Research ATTN: Dr. Michael McKissick 800 N. Quincy St. Arlington, Virginia 22217	1
6.	Chief of Naval Research ATTN: Dr. Raymond Fitzgerald 800 N. Quincy St. Arlington, Virginia 22217	1
7.	Eugene W. Brown NAVOCEANO Code 7300 Bay St. Louis, Missouri 39522	1
8.	Commanding Officer ATTN: Dr. James Andrews Naval Ocean Research and Development Activity NSTL Bay St. Louis, Missouri 39522	1
9.	LCDR M. K. Hedrick, U.S.N. 5313 Cerino Court Virginia Beach, Virginia 23464	1

END

FILMED

6-85

DTIC